A *Histoplasma capsulatum* lipid metabolic map identifies antifungal targets and virulence factors

Daniel Zamith-Miranda[1,2]*, Heino M. Heyman[3]*, Meagan C. Burnet[3]*, Sneha P. Couvillion[3], Xueyun Zheng[3], Nathalie Munoz[4], Jennifer E. Kyle[3], Erika M. Zink[3], Karl K. Weitz[3], Kent J. Bloodsworth[3], Geremy Clair[3], Jeremy D. Zucker[3], Jeremy R. Teuton[3], Samuel H. Payne[5], Young-Mo Kim[3], Morayma Reyes Gil[6], Erin S. Baker[7], Erin L. Bredeweg[4], Joshua D. Nosanchuk[1,2] and Ernesto S. Nakayasu[3,#]

[1]Department of Microbiology and Immunology and [2]Division of Infectious Diseases, Department of Medicine, Albert Einstein College of Medicine, Bronx, New York, USA; [3]Biological Sciences Division, Pacific Northwest National Laboratory, Richland, Washington, USA; [4]Environmental and Molecular Sciences Laboratory, Pacific Northwest National Laboratory, Richland, Washington, USA [5]Department of Biology, Brigham Young University, Provo, UT, USA; [6]Hematology Laboratory, Department of Pathology, Albert Einstein College of Medicine, Bronx, New York, USA; [7]Department of Chemistry, North Carolina State University, Raleigh, North Carolina, USA;.

*These authors equally contributed to this work

[#]To whom correspondence should be addressed.
Ernesto S. Nakayasu
Biological Science Division
Pacific Northwest National Laboratory
902 Battelle Boulevard
PO Box 999 MS-IN K8-98
Richland, WA, 99352, USA
Phone: +1(509) 371-6708
e-mail: ernesto.nakayasu@pnnl.gov

Running title: *H. capsulatum* lipid metabolism

Keywords: *Histoplasma capsulatum*, lipid metabolism, drug target, platelet-activating factor, multi-omics analysis

Abstract

Lipids play a fundamental role in fungal cell biology, being components of the cell membrane as well as targets of antifungal drugs. A deeper knowledge of lipid metabolism is key for developing new drugs and a better understanding of fungal pathogenesis. Here we built a comprehensive map of the *Histoplasma capsulatum* lipid metabolic pathway by integrating proteomic and lipidomic analyses. The map led to the identification of both the fatty acid desaturation and the sphingolipid biosynthesis pathways as targets for drug development. We also found that *H. capsulatum* produces analogs of platelet-activating factor, a potent regulator of the human immune response. The *H. capsulatum* platelet-activating factor analogs induced platelet aggregation and stimulated the production of the cytokines interleukin-10 and tumor necrosis factor-α by J774 macrophages. Overall, this lipid metabolic map revealed pathways that can be targeted for drug development, in addition to identifying a regulator of the host immune response.

Introduction

Fungal diseases affect more than 1 billion people and cause 1.6 million deaths every year (1). *Histoplasma capsulatum*, the causative agent of histoplasmosis, is an important pathogen in this context, being associated with HIV infections and a major cause of morbidity and mortality worldwide (2). A 2018 CDC report, reviewed hospitalization data from 2011-2014 in only 12 states in the US and identified 3,409 cases of histoplasmosis with a 7% mortality rate (3). Serological surveys have shown that sera from 60-90% of individuals are reactive to the *H. capsulatum* antigen histoplasmin in communities surrounding the Mississippi and Ohio basins, suggesting that epidemiological numbers of the disease could be underestimated (4, 5). Histoplasmosis treatment relies on only a few antifungal drugs, but the increasing number of resistant strains is a major public health concern (6, 7). The absence of immunotherapies and the fact that the newest class of antifungal drugs, echinocandins, has already been available for two decades, make the development of new therapies a high priority. A major hurdle in developing new drugs is the limited knowledge about the detailed metabolic reactions and mechanisms of pathogenesis of this microbe.

Lipids have essential roles in many biological processes and the biosynthetic pathways of fungal lipids diverged from metazoan pathways, which makes them obvious antifungal drug targets (8). Indeed, two classes of current antifungal drugs target lipid biosynthesis: 1) polyenes, including amphotericin B and nystatin, bind to ergosterol causing increased fungal cell membrane permeability and loss of intracellular constituents; and 2) azoles, such as voriconazole, itraconazole and fluconazole, inhibit the cytochrome P-450-dependent 14α-sterol demethylase, which is an enzyme of the ergosterol biosynthetic pathway (8, 9). More recently, glucosylceramide, a type of sphingolipid that is critical for infection of many fungal species, has been validated as a drug target in *Cryptococcus neorformans* (10, 11). Lipids have also been characterized as important molecules for fungal infections (12). For instance, glycolipids, sterols, as well as the chain length and level of desaturation of fatty acids play a role in pathogenesis (11, 13-18). Not only the specific lipid species but how they are organized into larger structures are also important for virulence. For instance, ergosterol-dependent microdomains have a crucial role in infectivity (19, 20). The role of lipids in virulence opens an opportunity to design drugs that target pathogenesis processes rather than the viability of fungal cells (21).

There is limited information about *H. capsulatum* lipid composition and function. The levels of *H. capsulatum* phosphatidylcholine correlate with its virulence (22). Similarly, perturbations in *H. capsulatum* membrane lipids reduce virulence (14, 23) and alterations in a

delta-9 fatty acid desaturase gene enhance temperature sensitivity (24). Also, unsaturated fatty acids decrease in aged yeast cells (25). In terms of sphingolipids, *H. capsulatum* also produces glucosylceramides, inositolphosphorylceramides and galactosyl-dimannosyl-inositolphosphorylceramides, which are components of membrane microdomains and are important for infection (20, 26, 27). Considering the importance of lipids, we reasoned that a deeper characterization of *H. capsulatum* lipid metabolism would result in the discovery of virulence factors and drug targets. In this study, we performed an in-depth characterization of the *H. capsulatum* lipid biosynthetic pathway by profiling its lipids and the associated proteins, which were integrated into a metabolic map. By comparing our results to *Saccharomyces cerevisiae* and humans, we show unique features of the lipid biosynthetic pathway of *H. capsulatum* that can be targeted for drug development. This analysis also led to the discovery that *H. capsulatum* produces analogs of platelet-activating factor (PAF), which are biologically active and regulate different aspects of the human immune response.

Results

Proteomic and lipidomic analyses and overview of the *H. capsulatum* lipid metabolism

To determine the global landscape of the lipid metabolic pathway of *H. capsulatum* we performed comprehensive lipidomic and proteomic analyses. Samples were extracted using two different methods and submitted to chromatographic separation before being analyzed by mass spectrometry. Paired global lipidomics and proteomics analyses were performed by submitting the samples to simultaneous metabolite, protein and lipid extraction (MPLEx)(28) (Fig. 1a). For complementary analyses of sterols, fatty acids and phospholipids, yeast cells were extracted with two rounds of organic solvent extraction, followed by a solid phase fractionation in a silica 60 column (Fig. 1a). The extracted fractions were analyzed by either gas chromatography-mass spectrometry (GC-MS) (sterols and fatty acids) or liquid chromatography-tandem mass spectrometry (LC-MS/MS) (sphingolipids, glycerolipids, phospholipids and proteins) (Fig. 1a).

The combined analysis identified 371 unique lipid species from 5 major lipid categories (fatty acids, sterols, glycerolipids, sphingolipids and glycerophospholipids (phospholipids + lysophospholipids)) that were subdivided into 19 subclasses (Fig. 1b and Supplementary Tab. 1-8). The most diverse subclasses of lipids in terms of number of identified lipids were triacylglycerols (TG), phosphatidylcholines (PC) and phosphatidylethanolamine (PE) with 130, 57 and 51 individual species, respectively (Fig. 1b). The proteomic analysis led to the identification of 3,215 proteins (Supplementary Tab. 9). To provide a measurement of the protein abundances in the cells, we calculated the relative copy number of each protein and scaled them into high, moderate, low and very low abundance (Fig. 1c), using a scale similar to one previously described (29). To validate this scale, we performed a function-enrichment analysis using the KEGG annotation to check the abundance of different pathways. As expected, glycolysis/gluconeogenesis and tricarboxylic acid (TCA) cycle were overrepresented among the highly abundant proteins, whereas DNA replication, nicotinate and nicotinamide metabolism, and basal transcription factors were enriched in moderate, low and very low abundance levels, respectively (Fig. 1d). The same scale showed that fatty acid metabolism was enriched in highly abundant proteins, whereas steroid biosynthesis proteins were mainly present in moderate abundance (Fig. 1c-d). Glycerophospholipid and sphingolipid metabolism proteins were not concentrated in a single abundance level and were spread mostly between moderate and low abundant levels (Fig. 1c-d). The abundance levels of the proteins were directly proportional to each type of lipid in the cellular membrane. For instance, the proteins of fatty acid and steroid (the building blocks of the cell membrane) metabolism were more abundant compared to proteins of the glycerophospholipid, ether lipid or sphingolipid

metabolism, which are responsible for the synthesis lipids from specific lower-abundance classes (Fig. 1d).

Lipid biosynthesis and remodeling map of *H. capsulatum*

To provide a global view of *H. capsulatum* lipid metabolism we built a map including lipid biosynthesis and remodeling reactions. The map was constructed based on a previous publication (30) and conserved metabolism between *H. capsulatum* vs. *S. cerevisiae* and *Cryptococcus neoformans*, the best characterized fungal organisms in terms of lipid metabolism (Supplementary Tab. 10). The *H. capsulatum* map was integrated with the relative abundance of the lipid species within the same subclass and the protein abundances (Fig. 2). In terms of fatty acids, lipids containing 16 and 18 carbons were the most abundant. Consistent with figure 1D, 5 out of 10 proteins of this pathway were highly abundant (Fig. 2). Similarly, 13 of the 23 sterol biosynthesis proteins had moderate abundance, with ergosterol being the most abundant product (Fig. 2). In the sphingolipid pathway, ceramides (Cer), hexosylceramide (HexCer), and inositolphosphoceramides (PI_Cer) were the detected lipid species (Fig. 2). Out of the 9 proteins detected in the proteome, 3 had low abundance, 5 had moderate abundance and 1 was highly abundant (Fig. 2). The number of low abundant proteins does not necessary mean that the pathway has low activity. For instance, one low abundant protein had more abundant paralogues with the same function (Lcb2 vs. Lcb1), and the other two proteins regulate the specific modification of the head group of HexCer (Fig. 2). In terms of glycerolipids, diacylglycerols (DGs) and TGs were identified, being the proteins from this pathway that were present at moderate (2), low (3) and very low abundance (1) (Fig. 2). Like the free-fatty acid composition, the most abundant species of DGs and TGs had fatty acyl groups with either 16 or 18 carbons attached to them (Fig. 2). Consistent to the glycerolipids, all the different glycerophospholipid classes had species bearing C16 and C18 as the most abundant in each (Fig. 2).

We further curated the map by studying the substrates and products of the acyltransferase Ale1 (also known as lysophosphatidylcholine (LPC) acyltransferase 1 – LPT1). A lipidomic analysis was performed in the *Lpt1* knockout strain of *S. cerevisiae* complemented or not with the *H. capsulatum* (*Hc-Lpt1*) orthologue (53% similarity to *S. cerevisiae Lpt1* – *Sc-Lpt1*), using a plasmid with a galactose-inducible promoter. Both gene knockout and recombinant expression were validated by proteomic analysis (Fig. 3a). As expected, the Sc-LPT1 specific peptide DISASSPNLGGILK was detected in wild-type *S. cerevisiae*, in both glucose- and galactose-supplemented media (Fig. 3a). The Hc-LPT1-specific peptide

LTAFCWNVHDGR was detected only in complemented strains that were grown in galactose-supplemented medium (Fig. 3a). The analysis showed that Hc-LPT1 complementation increased the abundances of 60 lipids, including phosphatidic acid (PA), PC, PE, phosphatidylinositol (PI), PS, DG, TG, Cer and mannosyl-inositolphosphoceramide (MIPC) (Fig. 3b-d, Supplementary Table 11). The Hc-LPT1 complementation also significantly reduced the levels of 77 lipids, including 5 LPC, 3 lysophosphatidylethanolamines (LPE), 2 sphinganines and 3 diacylglycerols (Supplementary Tab. 12). On the other hand, disruption of the Sc-LPT1 gene reduced the levels of 30 potential products, including PC, PE, PI, PS and TG. Notably, the proportion of acylated products between the LPT1 from the two species was very different, being PC, PE, PI and PS being more acylated by the *S. cerevisiae* ortholog and PA, DG, TG, Cer and MIPC by the *H. capsulatum* counterpart (Fig. 3D, Supplementary Tab. 13). The Sc-LPT1 showed a preference to produce lipid species containing short fatty acyl chains, with all the identified products having chains with ≤ 14 carbons (Fig. 3c). Complementation with *Hc-Lpt1* gene showed a different phenotype, as this orthologue produced lipid species containing odd-carbon number (C15 and C17) and longer (≥C18) fatty acyl chains (Fig. 3e). Overall, the map provides a global view of lipids being produced by *H. capsulatum* along with catalytic enzymes.

Divergent lipid metabolic pathways as drug targets

We next focused on pathways that could be targeted for antifungal chemotherapies. We searched for divergent pathways comparing *H. capsulatum* with *S. cerevisiae* and humans as candidates for anti-*H. capsulatum* drug targets. The most divergent pathways were fatty acid and sphingolipid metabolism. We examined the distribution of fatty acyl chains that are incorporated into *H. capsulatum* and *S. cerevisiae*. The results showed that both fungi incorporate fatty acyl groups with different chain lengths into their lipids. *S. cerevisiae* incorporate significantly more fatty acyl chains with less than 16 carbons (by Fisher's exact test), whereas *H. capsulatum* has significantly more lipids with fatty acids longer than 17 carbons (Fig. 4a). In terms of unsaturation, *S. cerevisiae* had almost exclusively saturated lipids or fatty acyl chains with 1 double bound, whereas *H. capsulatum* also had fatty acyl chains with 2 or 3 double bonds (Fig. 4b-c). This is consistent to the fact that *S. cerevisiae* has only one fatty acid desaturase gene (delta-9 desaturase, also known as oleate synthase *Ole1*) in its genome. In addition to Ole1, *H. capsulatum* has a delta-12 desaturase (*FAD2*) and two uncharacterized desaturases (HCBG_08514 and HCBG_05092) that might be responsible for the conversion of C18:2 and C20:2 to C18:3 and C20:3, respectively (top left part of Fig. 2). Because the human genome lacks delta-9 and delta-12 desaturases (Fig. 4b), we decided to

test it as a potential drug target. We tested two fatty acid desaturase inhibitors, 10-thiastearic acid and thiocarlide, as growth inhibitors of *H. capsulatum* yeasts. 10-Thiastearic acid showed a minimum-inhibitory concentration (MIC) of 1.25 μM, whereas the thiocarlide MIC was 12.5 μM (Fig. 4d). To confirm that these compounds target fatty acid desaturases we performed a fatty acid analysis. Cells were grown for 48 hours with one half of the MIC and fatty acids were extracted, methylated and analyzed by GC-MS. 10-Thiastearic acid had no effect on the ratio between unsaturated and saturated fatty acids (Fig. 4e), suggesting that this compound might target other pathways rather than the fatty acid desaturation. As expected, thiocarlide reduced the C18:2/C18:0 peak area ratio from 11.4 to 8.5 (25% reduction), the C18:1/C18:0 ratio from 4.5 to 3.7 (18% reduction) and the C20:1/C20:0 ratio from 1.3 to 0.8 (39% reduction) (Fig. 4e). Conversely, the C16:1/C16:0 ratio had a slight increase from 0.036 to 0.044 (22% increase) (Fig. 4e). These results show that the unsaturated fatty acid pathway can be targeted for developing anti-histoplasmosis drugs.

Sphingolipid metabolism was another pathway that had major differences in *H. capsulatum* compared to *S. cerevisiae. H. capsulatum* produces hexosylceramides (glucopyranosylceramides)(27), which are absent in *S. cerevisiae.* Even though both fungi produce inositolphosphoceramides and mannosyl-inositolphosphoceramides, they branch into different products (Fig. 5a). Whereas *S. cerevisiae* mannosyl-diinositolphospho-ceramides as a final product, *H. capsulatum* produces galactosyl-dimannosyl-inositolphosphoceramides (31) (Fig. 5a). Also, *H. capsulatum* makes two major pools of ceramide (4-hydroxysphinganine and 9-methyl-4,8-sphingadienine) but *S. cerevisiae* only makes 4-hydroxysphinganine (27, 30). Compared to fungi, humans produce a very distinct profile of sphingolipids. Unlike end product monohexosylceramides of fungi, humans synthesize a much more complex set of glycosphingolipids, including globo, isoglobo, lacto and gangliosides (32) (Fig. 5a). Conversely, fungi produce inositolphosphoceramides and their glycosylated derivates, which are absent in humans. Humans also produce sphingomyelins, which are absent fungi (Fig. 5a). The sphingolipid pathway can therefore be an excellent drug target due to these major differences in composition compared to humans. We performed a proof-of-concept by inhibiting the first enzyme of the sphingolipid biosynthesis, serine-palmitoyltransferase, with myriocin. Myriocin had a MIC of 30 nM (Fig. 5b). To confirm that myriocin targets the sphingolipid pathway, lipidomic analysis was performed on cells grown with one half of the MIC for 48 hours. As expected, the most abundant ceramide species, Cer(d18:1/24:0(2OH)) and Cer(d20:0/24:0), were reduced by 52% and 62%, respectively (Fig. 5c). As a control of a lipid from a unrelated class, the level of the most abundant DG, DG(16:0/18:2/0:0), increased by 51% (Fig. 5c). These

results validate the sphingolipid pathway as a potential target for developing anti-*H. capsulatum* drugs.

Discovery and validation of platelet-activating factor analogs in *H. capsulatum*

One unique lipid found in *H. capsulatum* was PC(16:2/2:0) (Fig. 6a and Supplementary Fig. 1). This lipid is analogous to the canonical platelet activating factor (PAF), a PC species containing ether-linked C16:0 chain in the sn1 position and acetyl group in the sn2 position (2-O-acetyl-1-O-hexadecyl-sn-glycero-3-phosphocholine – PC(O-16:0/2:0)) (Fig. 6a). PAF is a major regulator of the immune response in mammals (33). Therefore, we sought to further validate the structure of the *H. capsulatum* PAF analog. We searched for other lipids containing acetate as a fatty acyl chain in our lipidomics data and found another species, PC(16:1/2:0) (Supplementary Fig. 2). We next aimed to compare our molecule to a chemically synthesized standard, but unfortunately, PC(16:2/2:0) and PC(16:1/2:0) standards were not commercially available. The lack of knowledge on the double bond position prevented to synthesize the lipid containing the right fatty acyl group. We reasoned that *H. capsulatum* could be producing a saturated version of these lipid species (1-palmitoyl-2-acetyl-sn-glycerol-phophocholine – PC(16:0/2:0) – which is commercially available) (Fig. 6a), although in smaller amounts. The liquid chromatography-tandem mass spectrometry analysis found a peak with the expected *m/z* (mass to charge ratio) and retention time (Fig. 6b). To ensure that the sample background would not cause retention time shift, the sample was spiked with the standard and analyzed in parallel, which showed a consistent elution pattern with the standard alone and the endogenous species (Fig. 6b). Tandem mass fragmentation of this species showed a major fragment at *m/z* 184.07, derived from the breakage of the phosphocholine (ChoP) head group (Fig. 6c). Because tandem mass fragmentation of lipid species often generates only a few fragments, which is not optimum to confidently identify a molecule, we performed ion-mobility spectrometry coupled with mass spectrometry (IMS-MS) analysis. In the drift tube IMS-MS analyses performed, the ions were gently pulled by a weak electric field through the drift tube that is filled with nitrogen gas. As the ions collided with the gas molecules, they were separated based on their shape and size, allowing the separation of isobaric molecules which cannot be distinguished by *m/z* alone. *H. capsulatum* lipid extract was fractionated using a C18 column coupled to a HPLC system and fractions enriched with the lipids of interest were collected and analyzed by IMS-MS. The results showed a consistent drift time and collision cross section values when comparing the endogenous PC(16:0/2:0) to the synthetic standard (Fig. 6d). Overall, the retention time, high

mass accuracy, tandem mass fragmentation and drift time of the IMS-MS analyses consistently support the presence of acetylated PCs in *H. capsulatum*.

H. capsulatum PAF analogs are biologically active

To determine if the *H. capsulatum* PAF analogs have similar activity compared to the human canonical PAF, yeast lipid extracts were submitted to solid-phase extraction in a Silica 60 column and further separated by HPLC reverse phase chromatography using a C18 column. Each fraction was monitored by IMS-MS and the fractions containing *H. capsulatum* PAF analogs (fractions 8-10 in Fig. 7) were tested for their ability to aggregate platelets. Platelet aggregation was measured by impedance in whole blood. The results showed that the *H. capsulatum* fractions containing PAF analogs were active and promote the platelet aggregation, like the positive controls with the canonical PAF, PC(16:0/2:0) (acyl-PAF) and arachidonic acid (Fig. 7a-b).

We also tested the HPLC fractions enriched in *H. capsulatum* PAF analogs in their ability to induce cytokine production in J774 macrophage-like cells. The fractions induced a dose-dependent production of interleukin-10 (IL-10) and tumor necrosis factor (TNF)-α in pico to nanomolar range (estimated based on peak area relative to external standards), which is consistent to the activity of the PC(16:0/2:0) standard (Fig. 8a-b). The highest tested concentration of the lipid fractions and standard induced the production of a smaller amount of TNF-α (Fig. 8a-b), probably due to saturation or negative feedback mechanisms. The TNF-α production was inhibited by the PAF receptor antagonist WEB2086 (Fig. 8a-b), showing that *H. capsulatum* PAF analogs regulate J774 cells by engaging the PAF receptor.

Taken together our data show that *H. capsulatum* produces bioactive PAF analogs that activate platelets and induce cytokine production in host effector cells.

Discussion

Here we developed a global map of the *H. capsulatum* lipid metabolism by integrating genomic, proteomic and lipidomic information, including relative abundances of proteins and lipids. We found an accordance of the protein abundance levels with their function in the lipid metabolism. For instance, the proteins involved in the synthesis of the major lipid components, the fatty acids and sterols, were enriched among the high and moderate abundant proteins, whereas the proteins related to the synthesis of specific lipid head groups were enriched in the low to very low abundant proteins. This might be a consequence of cell resource optimization as protein synthesis is one of the most energetically expensive tasks in cells (34). Our lipid map also showed that TG, PC and PE are the most diverse classes of lipids. This could reflect the abundance of these lipid classes, as they are the most abundant ones(35). Our results show that the diversity of TG, PC and PE species could be due to fatty acid remodeling, as these lipids are products of the LPT1 acyltransferase. LPT1 transfers a variety of fatty acyl chains, including odd-carbon chain (C15 and C17) and long chain (≥C18) fatty acids. Our experiments with LPT1 also helped to curate the lipid map since the *S. cerevisiae* orthologue has a different specificity for substrates, that being a major impact in producing phospholipids with short fatty acyl chains. In *S. cerevisiae*, LPT1 has been shown *in vitro*, using radioactive precursors to acylated LPC, LPG, LPA, LPE, LPI and LPS (36). The acylation of LPA, a central precursor for all glycerolipids and glycerophospholipids, suggest that the LPT1 impact could be indirect. Therefore, further investigation will be needed to determine if this enzyme can directly acylate DG into TG.

We identified the fatty acid desaturation and the sphingolipid pathways as divergent points in the lipid metabolism pathways of *H. capsulatum* vs. *S. cerevisiae* and humans. We showed that these two pathways are potential targets for developing anti-histoplasmosis drugs. Thiocarlide (also known as isoxyl) is a potent inhibitor (nanomolar range) of *Mycobacterium turberculosis* delta-9 stearoyl desaturase and was used as a second line of anti-tuberculosis drugs in the 1960s (37, 38). However, despite its low toxicity, thiocarlide was not as effective during clinical trials, so is no longer used to treat patients (38-40). One possible explanation for the clinical trial failure is the poor solubility of the compound in water. Since then, other drug delivery vehicles have been tested with promising results *in vitro* (41). Delta-12 oleate desaturase has been validated as a drug target in trypanosomes (42). Indeed, both 10-thiastearic acid and thiocarlide inhibit *Trypanosoma cruzi* growth in low micromolar range (43), similar to the MICs for *H. capsulatum* (Fig. 4d). Although toxicity has not been tested directly with 10-thiastearate, its analog tetradecylthioacetic acid has a low toxicity in humans up to

1g/day (44), reinforcing the potential of this class of molecules as antimicrobial drugs. Our data showed that 10-thiastearate might target a different pathway rather than fatty acid desaturation, but it should still be considered a drug candidate due to its antifungal activity and possible low toxicity to humans.

We also performed a proof-of-concept that sphingolipids are promising targets for anti-histoplasma drug development by inhibiting the first step of the sphingolipid pathway with myriocin. Myriocin kills *Candida albicans* and *Aspergillus fumigatus* in micromolar concentrations (45, 46). *H. capsulatum* is more sensitive to myriocin as its MIC was 30 nM (Fig. 5b). Unfortunately, myriocin has immunosuppressant activity (47, 48), but this has been explored for simultaneously killing the fungus and reducing the pathogenic inflammation of the lungs in cystic fibrosis mice infected with *A. fumigatus* (49). The fact the *de novo* sphingolipid synthesis is essential for *H. capsulatum* opens the opportunity to explore other inhibitors of serine palmitoyltransferase, or other enzymes in the pathway. Indeed, other enzymes of the fungal sphingolipid pathway have been validated as a drug target. In *C. neoformans*, acylhydrazones have been shown to be potent inhibitors of the glucosylceramide synthesis (nanomolar range) and excellent antifungal drug candidates (10, 50).

Our study also led to the identification of PAF analogs in *H. capsulatum*. Such analogs were previously described in *S. cerevisiae*, which is synthesized by the acyltransferase LTP1 (36, 51). We were able to validate these findings by analyzing the Sc-LPT1 knockout strain, which had the production of PC(16:1/2:0) drastically reduced (Supplementary Fig. 3). Unfortunately, the *H. capsulatum* preferred substrate LPC(16:2) is not present in *S. cerevisiae*, due to the lack of additional desaturases in this species. Complementation of *S. cerevisiae* knockout strain with the Hc-LPT1 orthologue significantly increased the abundance of PC(16:1/2:0) (Supplementary Fig. 3). Therefore, it is possible that LPT1 is PAF synthase in *H. capsulatum*. However, this and other possibilities, such as PAF being synthesized by a different acyltransferase, need to be confirmed with more experiments. The *H. capsulatum* PAF analogs induced platelet activation and PAFR-dependent cytokine production. PAF has a variety of functions in regulating the host immune response and it has been shown to be essential for neutrophil recruitment to the site of infection in histoplasmosis (52). Since acyl-PAF has pro- and anti-PAF activity depending on the physiological condition (53), it is possible that the *H. capsulatum* PAF analogs play a role in controlling the immune response against histoplasmosis.

In conclusion, here we built a detailed map of *H. capsulatum* lipid metabolism. Our data identified regions of the *H. capsulatum* lipid metabolic pathway that can be targeted for drug

development and led to the characterization of lipid species that have immunoregulatory activities.

MATERIAL AND METHODS

Fungal cell culture

Histoplasma capsulatum G217B strain was purchased from the American Type and Culture Collection (ATCC, Manassas, VA) and grown in yeast form at 37°C in Ham's F12 medium as previously described (54). *S. cerevisiae* (MATalpha background) deficient LPT1 gene and wild-type strains were purchased from Dharmacon (Lafayette, CO). The strains were transformed by a lithium-acetate-heat shock method with a plasmid containing the Hc-LPT1 gene (Uniprot ID C0NZS2) that was codon optimized, synthesized and clone into the Gal-inducible plasmid pESC-URA by GenScript (Piscataway, NJ). The cells were cultivated in YNB medium containing leucine, lysine, histidine and uracil, further supplemented with of glucose or galactose at 28 °C with shaking at 200 rpm until the culture reached an OD600 of 0.8-1.0. Cells were harvested by centrifuging at 2000 x *g* for 2 min and washed twice with PBS. All the sample preparation and analysis were done in 4 replicates and in a randomized order to ensure the biological significance and prevent batch effects.

Sample extraction and fractionation on Silica 60 column

Samples were extracted using two different approaches. For global proteomics and lipidomics analyses, samples were submitted to Metabolite, Protein and Lipid Extraction (MPLEx) as previously described (28). For the fractionation study, cells were suspended in 400 µL of water and transferred to PTFE-lined 13x100-mm Pyrex glass tubes (prewashed with chloroform:methanol (2:1, v:v) and chloroform:methanol:water (1:2:0.8, v:v:v)) containing 200 µL of silica/zirconia beads(55). 1 mL of methanol and 0.5 mL of chloroform to form chloroform:methanol:water (1:2:0.8, v:v:v) solution and extracted by vortexing for 2 minutes followed by centrifugation for 10 minutes at 1,800 x *g* at room temperature. The supernatants were collected into clean glass tubes. Samples were additionally extracted twice with 1 mL of chloroform:methanol (2:1, v:v) and once with 1 mL of chloroform:methanol:water (1:2:0,8, v:v:v), and the supernatants were pooled together then dried in a vacuum centrifuge. Extracted lipids were fractionated into neutral lipids, fatty acids and phospholipid fractions using Silica 60 columns(56) and dried in a vacuum centrifuge.

High performance liquid chromatography (HPLC) fractionation of phospholipids

The phospholipid fraction from the Silica 60 separation was reconstituted in 2 mL methanol:dichloromethane (8:2), centrifuged and the supernatant was loaded (100 µL) onto a

reverse-phase column (Kinetex®, Torrance, CA, 150 x 4.6 mm, 2.6 µm, C18, 100 Å,) coupled to a 1200 Agilent HPLC and fraction collector (Agilent™, Santa Clara, CA, USA). The samples were loaded in the column equilibrated with 60% solvent A (60:40 acetonitrile:water + 10mM ammonium acetate) in 40% solvent B (90:10 isopropanol:acetonitrile + 10mM ammonium acetate) and the elution was performed at a flow rate of 0.5 mL/min using the following gradient: 40-50%B in 2 min, 50-60% B in 1 min, 60-70% B in 9 min, hold in 70% B for 3 min, 70-78% B in 2 min, 78-85% B in 2 min, 85-99%B in 6 min and hold at 99% B for 3 min. Eluting lipids were monitored by electrospray ionization mass spectrometry (LTQ™ Linear Ion Trap Mass Spectrometer, Thermo Scientific™, Waltham, MA, USA) with 26 fractions collected in regular intervals of 1 min from RT 2.5 min – 28.5 min. Fractions from 18 fractionation runs were dried in a vacuum centrifuge and dissolved in appropriate solvent for subsequent analyses.

Proteomic analysis

Extracted proteins were suspended in 100 µL of 8 M urea in 50 mM NH_4HCO_3 and protein concentration was determined by a BCA protein assay (Thermo Scientific, Rockford, IL). Samples were digested as previously described (54) and desalted using 1 mL Discovery C18 SPE columns (Supelco, Bellefonte, PA). Digested peptides were suspended in water, quantified by BCA assay and had their concentrations adjusted to 0.1 µg/µL with water. A total of 500 ng of peptides were direct injected onto the analytical column. The analytical column used was prepared in-house by slurry packing 3-µm Jupiter C18 stationary phase (Phenomenex, Torrence, CA) into a 70-cm long, 360 µm OD x 75 µm ID fused silica capillary tubing (Polymicro Technologies Inc., Phoenix, AZ). The column was coupled to a Waters M-ClassTM UPLC system (Millford, MA) connected with a Q-Exactive Plus hybrid quadrupole/Orbitrap mass spectrometer from Thermo Fisher Scientific (San Jose, CA). Mobile phases consisted of 0.1% formic acid in water (MP-A) and 0.1% formic acid in acetonitrile (MP-B). The gradient elution, and column regeneration profile was as follows (min:%MP-B); 0:0.1, 4.0:8, 36:12, 135:30, 175:45, 180:95, 190:95, 195:1. Data acquisition (180 min) was started at the end of the sample loading period (20 min). The analytical column was coupled to the Q-Exactive using a home-built nanospray adapter interface with 2.2 kV applied to achieve electrospray ionization. The MS inlet was maintained at a temperature of 275 °C. A precursor scan was performed from *m/z* 400 to 2000 at a resolution of 35k at *m/z* 400 and an automatic gain control (AGC) of 3e6. Operated in data dependent mode, the top 12 most intense ions from the precursor scan were selected for high energy collision dissociation (HCD) MS/MS at a resolution of 17.5k, AGC of 1e5, isolation window of 2 m/z, and a max ion time of 100 ms. Only ions identified as having a +2

charge or higher were subjected to HCD and subsequently excluded from further analysis for 30 sec thereby allowing for deeper coverage.

LC-MS/MS data were analyzed with MaxQuant software (v.1.5.5.1) by searching against the *H. capsulatum* G186AR (downloaded August 15, 2016) and *S. cerevisiae* S288c (downloaded January 11, 2018) sequences from Uniprot Knowlegdgebase, considering protein N-terminal acetylation and oxidation of methionine as variable modifications, and cysteine carbamidomethylation as a fixed modification. The parent ion mass tolerance was set at 20 and 4.5 ppm for the first and main peptide searches, whereas the fragment mass tolerance was set as 20 ppm for both searching rounds. Tryptic digestion was required for peptide termini and up to 2 missed cleavage sites were allowed per peptide. Protein abundances were estimated by the intensity based absolute quantification (iBAQ) method (57). The intensities were normalized by the total iBAQ sum of each sample and expressed as relative number of protein copies (percentage from total). Proteins were classified according to their abundance converting number of copies described by Beck et al. (29) to relative number of protein copies (%). Function-enrichment analysis was performed as described previously (58).

Lipid analysis by liquid chromatography-tandem mass spectrometry

Total lipid extracts and phospholipid fraction from the Silica 60 column were resuspended in methanol and subjected to LC-MS/MS analysis as previously described (59). To assess the technical variability, we spiked in the SPLASH Lipidomix standard (Avanti Polar), which contains a mix isotopically labeled lipids. Lipid species were identified using LIQUID and manually inspected for validation. The features of the identified lipid species were extracted and aligned using Mzmine (60). For comparative purposes, lipids were considered significantly different with $p \leq 0.05$ by *t*-test considering equal variance and unpaired samples. The distribution of fatty acyl groups was done by counting individual fatty acyl groups and were considered significantly different with a $p \leq 0.05$ by Fisher's exact test.

Lipid Analysis by ion mobility spectrometry-mass spectrometry (IMS-MS)

HPLC-fractionated fractions were suspended in methanol and analyzed on an Agilent 6560 IMS-QTOF MS platform (Agilent Technologies, Santa Clara, CA) (61). For IMS measurements, ions were generated by an electrospray ionization source, passed through the glass capillary, focused and accumulated in the ion funnel before being pulsed into the IMS drift tube filled with ~ 3.95 torr of nitrogen gas, where they traveled under the influence of a weak electric field (10-20 V/cm). Ions exiting the drift tube are then refocused by a rear ion funnel prior

to being detected by QTOF MS, and their arrival times were recorded. Collision-cross section (CCS) which contains information of molecule size and shape can be determined from the data acquired under different electric fields. The Agilent IM-MS Browser software was used to process IMS data, extract IMS profiles and calculate CCS values. Candidate phospholipid species were matched to standards based on their CCS values and MS/MS spectra.

Fatty acid and sterol analyses

Fatty acid fractions from the silica 60 column fractionation were resuspended in 0.5 mL of anhydrous methanolic HCl (1.2 N), sealed and incubated for 1 h at 100°C. After cooling, 0.5 mL of water was added and the fatty acid methyl esters (FAMEs) were extracted by adding 0.5 mL hexane and vortexing the samples. Sterol fractions were derivatized with N-methyl-N-(trimethylsilyl)trifluoroacetamide (MSTFA) (Sigma-Aldrich) and trimethylchlorosilane (TMCS) (Sigma-Aldrich) as described in details elsewhere(62). Derivatized FAMEs and sterols were then analyzed by GC-MS. For the background referencing and retention time calibration, blanks and FAME standard mix (C8-28) (Sigma-Aldrich) were also analyzed. Analyses were performed in an Agilent GC 7890A using a HP-5MS column (30 m × 0.25 mm × 0.25 µm; Agilent Technologies, Santa Clara, CA) coupled with a single quadrupole MSD 5975C (Agilent Technologies). For each analysis 1 µL of sample was injected (splitless) into the injection port with constant temperature at 250°C. The GC analysis started with an initial oven temperature fixed at 60°C for 1 minute after injection, and then the temperature was increased to 325°C at a rate of 10°C/minute, and finished with a 5-minute hold at 325°C. The data files were calibrated and deconvoluted with Metabolite Detector as stated previously(63). Molecules were identified by library matching against the FiehnLib (64) with some in-house added entries. Unidentified chromatographic features were also searched against the Wiley Fatty Acids Methyl Esters Mass Spectral Database and the NIST17 GC-MS spectral library.

Construction of the *H. capsulatum* lipid metabolic map

We have built a preliminary G217B lipid map with a tool name VANTED v2.6.5(65), using the *S. cerevisiae* model (30) as a starting point. Enzyme orthologues were identified by blasting *S. cerevisiae* and *C. neoformans*, two of the best characterized fungi in terms of lipid metabolism (30, 66). The map was integrated with abundance level of lipids using their relative mass spectrometry intensities within the same lipid class.

Evaluation of lipid biosynthesis pathways on *H. capsulatum* growth

The tested compounds (myriocin, 10-thiastearic acid and thiocarlide) were serially diluted in round bottom 96-well plates. *H. capsulatum* yeast cells were washed with PBS and suspended in Ham's F12. Yeast cells were added in 4 replicates to the drug-containing plates at a final cellular density of 2.5 x 10^4 cells per mL. The plates were incubated at 37 ºC under constant shaking for 7 days until the optical analysis of growth. The drug concentration present in the set of replicates with no visual growth was considered the MIC for each of the drugs. To evaluate the effect of lipid synthesis inhibition of *H. capsulatum*, 10^6 cells/mL were incubated in Ham's F12 in the presence or absence of myriocin, 10-thiasteric acid and thiocarlide in half of the evaluated MIC for each drug. The cultures were kept at 37ºC shaking at 250 rpm for 48 hours. Cells were extensively washed with ice-cold PBS and pellets were frozen for further lipid extraction and subsequent fatty acid and lipidomics analyses. This experiment was performed in triplicates.

Platelet aggregation assay

Platelet-rich and platelet-depleted plasma were obtained from human blood by differential centrifugation. Platelet aggregation was measured in a Chrono-Log 700 aggregometer by impedance in whole blood.

Treatment of macrophages with *H. capsulatum* lipid fractions

J774 macrophage-like cell line was cultivated in DMEM medium containing 10% FBS at 37°C and 5% CO_2 atmosphere. Cells were then treated for 24 hours with lipids fractionated by HPLC and resuspended in methanol. Due to the lack of the exact concentration of the lipid fractions, these were tested in 4 dilutions: 10^{-3}, 10^{-4}, 10^{-5} and 10^{-6}. Control treatments were carried in the presence or absence of the PAF receptor antagonist WEB 2086, and vehicle only (same amount as in the highest concentration of the fractions – 0.1%). After treatment TNF-α and IL-10 were measured by ELISA (B&D). Results were analyzed with GraphPad (Prism) and were considered significant with $p \leq 0.05$ by ANOVA followed by Tukey's multiple comparison test.

AUTHOR CONTRIBUTIONS

D.Z.M., H.M.H., M.C.B., J.D.N and E.S.N. designed the research. D.Z.M. performed the *H. capsulatum* growth, drug testing and cytokine experiments. H.M.H., M.C.B., E.M.Z., J.E.K., K.K.W., E.L.B. and K.J.B. performed the lipidomics and proteomics experiments. E.L.B. performed the genetic engineering of the *S. cerevisiae* strains. M.C.B., H.M.H., N.M.M. and Y.M.K. performed the gas chromatography-mass spectrometry analyses. E.S.N., G.C., J.D.Z., J.R.T. build the lipid metabolic map. X.Z. and E.S.B. performed the ion mobility-mass spectrometry analysis. M.R.G. performed the platelet aggregation analysis. D.Z.M., H.M.H., M.C.B., S.P.C., X.Z., E.S.B, J.E.K., S.H.P., Y.M.K., M.R.G., J.D.N., and E.S.N. analyzed the data. M.R.G., E.S.B, S.H.P., J.D.N and E.S.N. contributed with reagents and resources. D.Z.M., H.M.H, M.C.B. and E.S.N. wrote the manuscript with inputs from the other authors. All the authors read and approved the final version of the manuscript.

CONFLICTS OF INTEREST

The authors declare no financial conflicts of interest.

Acknowledgments

The authors thank Drs. Igor Almeida, Rosa Maldonado, Milene Carmes Vallejo, Charles Ansong and Joshua Adkins for insightful discussions. Joshua D. Nosanchuk and Ernesto S. Nakayasu were supported by NIH R21 AI124797. Erin L. Bredeweg, Ernesto S. Nakayasu, Jennifer Kyle were supported by a Laboratory Directed Research and Development project from Pacific Northwest National Laboratory (PNNL). Erin S. Baker would also like to acknowledge support from NIEHS P42 ES027704. Parts of this work were performed in the Environmental Molecular Science Laboratory, a U.S. Department of Energy (DOE) national scientific user facility at PNNL in Richland, WA.

Data availability. Proteomics data were deposited into Pride repository (www.ebi.ac.uk/pride) under accession number PXD017734.

Username: reviewer86800@ebi.ac.uk

Password: 9cZs0O1G

References

1. Bongomin F, Gago S, Oladele RO, & Denning DW (2017) Global and Multi-National Prevalence of Fungal Diseases-Estimate Precision. *J Fungi (Basel)* 3(4).
2. Chu JH, Feudtner C, Heydon K, Walsh TJ, & Zaoutis TE (2006) Hospitalizations for endemic mycoses: a population-based national study. *Clin Infect Dis* 42(6):822-825.
3. Armstrong PA*, et al.* (2018) Multistate Epidemiology of Histoplasmosis, United States, 2011-2014. *Emerg Infect Dis* 24(3):425-431.
4. Antinori S (2014) Histoplasma capsulatum: more widespread than previously thought. *Am J Trop Med Hyg* 90(6):982-983.
5. Benedict K & Mody RK (2016) Epidemiology of Histoplasmosis Outbreaks, United States, 1938-2013. *Emerg Infect Dis* 22(3):370-378.
6. Goughenour KD & Rappleye CA (2017) Antifungal therapeutics for dimorphic fungal pathogens. *Virulence* 8(2):211-221.
7. Parente-Rocha JA*, et al.* (2017) Antifungal Resistance, Metabolic Routes as Drug Targets, and New Antifungal Agents: An Overview about Endemic Dimorphic Fungi. *Mediators Inflamm* 2017:9870679.
8. Pianalto KM & Alspaugh JA (2016) New Horizons in Antifungal Therapy. *J Fungi (Basel)* 2(4).
9. Ghannoum MA & Rice LB (1999) Antifungal agents: mode of action, mechanisms of resistance, and correlation of these mechanisms with bacterial resistance. *Clin Microbiol Rev* 12(4):501-517.
10. Mor V*, et al.* (2015) Identification of a New Class of Antifungals Targeting the Synthesis of Fungal Sphingolipids. *MBio* 6(3):e00647.
11. Rittershaus PC*, et al.* (2006) Glucosylceramide synthase is an essential regulator of pathogenicity of Cryptococcus neoformans. *J Clin Invest* 116(6):1651-1659.
12. Hogan LH, Klein BS, & Levitz SM (1996) Virulence factors of medically important fungi. *Clin Microbiol Rev* 9(4):469-488.
13. Fradin C, Bernardes ES, & Jouault T (2015) Candida albicans phospholipomannan: a sweet spot for controlling host response/inflammation. *Semin Immunopathol* 37(2):123-130.
14. Carratu L*, et al.* (1996) Membrane lipid perturbation modifies the set point of the temperature of heat shock response in yeast. *Proc Natl Acad Sci U S A* 93(9):3870-3875.
15. Nguyen LN, Trofa D, & Nosanchuk JD (2009) Fatty acid synthase impacts the pathobiology of Candida parapsilosis in vitro and during mammalian infection. *PLoS One* 4(12):e8421.
16. Nguyen LN, Gacser A, & Nosanchuk JD (2011) The stearoyl-coenzyme A desaturase 1 is essential for virulence and membrane stress in Candida parapsilosis through unsaturated fatty acid production. *Infect Immun* 79(1):136-145.
17. Singh A*, et al.* (2012) Methylation of glycosylated sphingolipid modulates membrane lipid topography and pathogenicity of Cryptococcus neoformans. *Cell Microbiol* 14(4):500-516.
18. O'Meara TR*, et al.* (2018) High-Throughput Screening Identifies Genes Required for Candida albicans Induction of Macrophage Pyroptosis. *MBio* 9(4).
19. Siafakas AR, Wright LC, Sorrell TC, & Djordjevic JT (2006) Lipid rafts in Cryptococcus neoformans concentrate the virulence determinants phospholipase B1 and Cu/Zn superoxide dismutase. *Eukaryot Cell* 5(3):488-498.
20. Tagliari L*, et al.* (2012) Membrane microdomain components of Histoplasma capsulatum yeast forms, and their role in alveolar macrophage infectivity. *Biochim Biophys Acta* 1818(3):458-466.

21. Rella A, Farnoud AM, & Del Poeta M (2016) Plasma membrane lipids and their role in fungal virulence. *Prog Lipid Res* 61:63-72.
22. Nielsen HS (1966) Variation in Lipid Content of Strains of *Histoplasma capsulatum* Exhibiting Different Virulence Properties for Mice. *Journal of bacteriology* 91(1):273-277.
23. Maresca B & Kobayashi G (1993) Changes in membrane fluidity modulate heat shock gene expression and produced attenuated strains in the dimorphic fungus *Histoplasma capsulatum*. *Archives of medical research* 24(3):247-249.
24. Gargano S, Di Lallo G, Kobayashi GS, & Maresca B (1995) A temperature-sensitive strain of *Histoplasma capsulatum* has an altered delta 9-fatty acid desaturase gene. *Lipids* 30(10):899-906.
25. Zarnowski R, Dobrzyn A, Ntambi JM, & Woods JP (2008) Neutral storage lipids of *Histoplasma capsulatum*: effect of culture age. *Curr Microbiol* 56(2):110-114.
26. Levery SB, Toledo MS, Straus AH, & Takahashi HK (2001) Comparative analysis of glycosylinositol phosphorylceramides from fungi by electrospray tandem mass spectrometry with low-energy collision-induced dissociation of Li(+) adduct ions. *Rapid Commun Mass Spectrom* 15(23):2240-2258.
27. Toledo MS, Levery SB, Suzuki E, Straus AH, & Takahashi HK (2001) Characterization of cerebrosides from the thermally dimorphic mycopathogen Histoplasma capsulatum: expression of 2-hydroxy fatty N-acyl (E)-Delta(3)-unsaturation correlates with the yeast-mycelium phase transition. *Glycobiology* 11(2):113-124.
28. Nakayasu ES*, et al.* (2016) MPLEx: a Robust and Universal Protocol for Single-Sample Integrative Proteomic, Metabolomic, and Lipidomic Analyses. *mSystems* 1(3).
29. Beck M*, et al.* (2011) The quantitative proteome of a human cell line. *Mol Syst Biol* 7:549.
30. Casanovas A*, et al.* (2015) Quantitative analysis of proteome and lipidome dynamics reveals functional regulation of global lipid metabolism. *Chem Biol* 22(3):412-425.
31. Guimaraes LL, Toledo MS, Ferreira FA, Straus AH, & Takahashi HK (2014) Structural diversity and biological significance of glycosphingolipids in pathogenic and opportunistic fungi. *Front Cell Infect Microbiol* 4:138.
32. Merrill AH, Jr. (2011) Sphingolipid and glycosphingolipid metabolic pathways in the era of sphingolipidomics. *Chem Rev* 111(10):6387-6422.
33. Prescott SM, Zimmerman GA, Stafforini DM, & McIntyre TM (2000) Platelet-activating factor and related lipid mediators. *Annu Rev Biochem* 69:419-445.
34. Metzl-Raz E*, et al.* (2017) Principles of cellular resource allocation revealed by condition-dependent proteome profiling. *Elife* 6.
35. Domer JE & Hamilton JG (1971) The readily extracted lipids of Histoplasma capsulatum and Blastomyces dermatitidis. *Biochim Biophys Acta* 231(3):465-478.
36. Tamaki H*, et al.* (2007) LPT1 encodes a membrane-bound O-acyltransferase involved in the acylation of lysophospholipids in the yeast Saccharomyces cerevisiae. *J Biol Chem* 282(47):34288-34298.
37. Phetsuksiri B*, et al.* (2003) Unique mechanism of action of the thiourea drug isoxyl on Mycobacterium tuberculosis. *J Biol Chem* 278(52):53123-53130.
38. Phetsuksiri B*, et al.* (1999) Antimycobacterial activities of isoxyl and new derivatives through the inhibition of mycolic acid synthesis. *Antimicrob Agents Chemother* 43(5):1042-1051.
39. Tousek J (1970) On the clinical effectiveness of Isoxyl. *Antibiot Chemother* 16:149-155.
40. Urbancik B (1970) Clinical experience with thiocarlide (Isoxyl). *Antibiot Chemother* 16:117-123.
41. Wang C & Hickey AJ (2010) Isoxyl particles for pulmonary delivery: In vitro cytotoxicity and potency. *Int J Pharm* 396(1-2):99-104.

42. Maldonado RA, Kuniyoshi RK, Linss JG, & Almeida IC (2006) Trypanosoma cruzi oleate desaturase: molecular characterization and comparative analysis in other trypanosomatids. *J Parasitol* 92(5):1064-1074.
43. Alloatti A, Testero SA, & Uttaro AD (2009) Chemical evaluation of fatty acid desaturases as drug targets in Trypanosoma cruzi. *Int J Parasitol* 39(9):985-993.
44. Pettersen RJ*, et al.* (2008) Pharmacology and safety of tetradecylthioacetic acid (TTA): phase-1 study. *J Cardiovasc Pharmacol* 51(4):410-417.
45. Kluepfel D, Bagli J, Baker H, Charest MP, & Kudelski A (1972) Myriocin, a new antifungal antibiotic from Myriococcum albomyces. *J Antibiot (Tokyo)* 25(2):109-115.
46. Perdoni F*, et al.* (2015) Antifungal activity of Myriocin on clinically relevant Aspergillus fumigatus strains producing biofilm. *BMC Microbiol* 15:248.
47. de Melo NR*, et al.* (2013) Myriocin significantly increases the mortality of a non-mammalian model host during Candida pathogenesis. *PLoS One* 8(11):e78905.
48. Strader CR, Pearce CJ, & Oberlies NH (2011) Fingolimod (FTY720): a recently approved multiple sclerosis drug based on a fungal secondary metabolite. *J Nat Prod* 74(4):900-907.
49. Caretti A*, et al.* (2016) Inhibition of ceramide de novo synthesis by myriocin produces the double effect of reducing pathological inflammation and exerting antifungal activity against A. fumigatus airways infection. *Biochim Biophys Acta* 1860(6):1089-1097.
50. Lazzarini C*, et al.* (2018) Acylhydrazones as Antifungal Agents Targeting the Synthesis of Fungal Sphingolipids. *Antimicrob Agents Chemother* 62(5).
51. Nakayama R, Kumagai H, & Saito K (1994) Evidence for production of platelet-activating factor by yeast Saccharomyces cerevisiae cells. *Biochim Biophys Acta* 1199(2):137-142.
52. Medeiros AI*, et al.* (2015) Impairment of neutrophil migration to remote inflammatory site during lung histoplasmosis. *Biomed Res Int* 2015:409309.
53. Chaithra VH*, et al.* (2018) Modulation of inflammatory platelet-activating factor (PAF) receptor by the acyl analogue of PAF. *J Lipid Res* 59(11):2063-2074.
54. Matos Baltazar L*, et al.* (2016) Antibody Binding Alters the Characteristics and Contents of Extracellular Vesicles Released by Histoplasma capsulatum. *mSphere* 1(2).
55. Vallejo MC*, et al.* (2012) Lipidomic analysis of extracellular vesicles from the pathogenic phase of Paracoccidioides brasiliensis. *PLoS One* 7(6):e39463.
56. Albuquerque PC*, et al.* (2008) Vesicular transport in Histoplasma capsulatum: an effective mechanism for trans-cell wall transfer of proteins and lipids in ascomycetes. *Cell Microbiol* 10(8):1695-1710.
57. Wilhelm M*, et al.* (2014) Mass-spectrometry-based draft of the human proteome. *Nature* 509(7502):582-587.
58. Baltazar LM*, et al.* (2018) Concentration-dependent protein loading of extracellular vesicles released by Histoplasma capsulatum after antibody treatment and its modulatory action upon macrophages. *Sci Rep* 8(1):8065.
59. Dautel SE*, et al.* (2017) Lipidomics reveals dramatic lipid compositional changes in the maturing postnatal lung. *Sci Rep* 7:40555.
60. Pluskal T, Castillo S, Villar-Briones A, & Oresic M (2010) MZmine 2: modular framework for processing, visualizing, and analyzing mass spectrometry-based molecular profile data. *BMC Bioinformatics* 11:395.
61. Zhang X*, et al.* (2016) SPE-IMS-MS: An automated platform for sub-sixty second surveillance of endogenous metabolites and xenobiotics in biofluids. *Clin Mass Spectrom* 2:1-10.
62. Kim YM*, et al.* (2013) Salmonella modulates metabolism during growth under conditions that induce expression of virulence genes. *Mol Biosyst* 9(6):1522-1534.
63. Hiller K*, et al.* (2009) MetaboliteDetector: comprehensive analysis tool for targeted and nontargeted GC/MS based metabolome analysis. *Anal Chem* 81(9):3429-3439.

64. Kind T, *et al.* (2009) FiehnLib: mass spectral and retention index libraries for metabolomics based on quadrupole and time-of-flight gas chromatography/mass spectrometry. *Anal Chem* 81(24):10038-10048.
65. Hartmann A & Jozefowicz AM (2018) VANTED: A Tool for Integrative Visualization and Analysis of -Omics Data. *Methods Mol Biol* 1696:261-278.
66. Munshi MA, *et al.* (2018) The Role of Ceramide Synthases in the Pathogenicity of *Cryptococcus neoformans*. *Cell reports* 22(6):1392-1400.

Figure legends

Fig. 1 | Proteomic and lipidomic analyses of *Histoplasma capsulatum* yeast cells. (a) Extraction procedure for lipidomics proteomics analyses. Yeast cells were extracted sequentially with chloroform:methanol (2:1, v:v) and chloroform:methanol:water (1:2:0.8, v:v:) and fractionated by Silica 60 solid phase extraction for sterol, free fatty acid and phospholipid analyses. Cells were also submitted to simultaneous metabolite, protein and lipid extraction (MPLEx) for global lipidomics and proteomics analyses. (**b**) Overall lipid coverage combining MPLEx and specific lipid extractions of *Histoplasma capsulatum*. (**c**) Protein abundance classification based on their relative copy numbers. (**d**) Function enrichment analysis based on the KEGG annotation of *H. capsulatum* proteins with different abundance levels. Abbreviations: C, chloroform; Cer, ceramide; CL, cardiolipin; DG, diacylglycerol; FA, fatty acid; HexCer, hexosylceramide; LPC, lysophosphatidylcholine, LPE, lysophosphatidylethanolamines, LPG, lysophosphatidylglycerol; LPI, lysophosphatidylinositol; LPS, lysophosphatidylserine; M, methanol; PA, phosphatidic acid; PC, phosphatidylinositol; PE, phosphatidylethanolamine; PG, phosphatidylglycerol; PI, phosphatidylinositol; PI_Cer, inositolphosphoceramide; PL, phospholipid; PS, phosphatidylserine; ST, sterol; TG, triacylglycerol; W, water.

Fig. 2 | Integrated metabolic map of *Histoplasma capsulatum* lipids and biosynthesis proteins. The map was built based on the genomic information along with proteomics and lipidomics data. Lipids abundances were normalized by the most intense signal in the mass spectrometry analysis within each lipid class, whereas the proteins were classified based on their relative copy number. For details about enzyme names and orthologues see table **S10**. Abbreviations: Cer, ceramide; CL, cardiolipin; DG, diacylglycerol; HexCer, hexosylceramide; LPC, lysophosphatidylcholine, LPE, lysophosphatidylethanolamines, LPG, lysophosphatidylglycerol; LPI, lysophosphatidylinositol; LPS, lysophosphatidylserine; M, methanol; PA, phosphatidic acid; PC, phosphatidylinositol; PE, phosphatidylethanolamine; PG, phosphatidylglycerol; PI, phosphatidylinositol; PI_Cer, inositolphosphoceramide; PL, phospholipid; PS, phosphatidylserine; TG, triacylglycerol.

Fig. 3 | Analysis of *Saccharomyces cerevisiae* (Sc) and *Histoplasma capsulatum* (Hc) lysophospholipid acetyltransferase LPT1 genes. The analysis was done in wild-type and LPT1-knockout (KO) (*Lpt1* -/-) *S. cerevisiae* strains complemented or not with the pESC-URA plasmid with Hc-LPT1 gene under galactose-inducible promoter. *S. cerevisiae* WT and LPT1-knockout (KO) strains were grown in YNB medium supplemented with of glucose (Glc) or galactose (Gal). (**a**) Protein abundance of Sc and Hc LPT1 proteins measured by the intensity of specific peptides in the LC-MS/MS analysis. Elongation factor Tu (TUF1) was used as a loading control. As expected, Sc LPT1 was only detected in the WT strain, whereas Hc LPT1 was detected only in strains transformed with the plasmid and induced with galactose. (**b-c**) Heatmaps of identified HcLPT1 (**b**) and ScLPT1 (**c**) products ($p \leq 0.05$ compared the complemented vs control strains (**b**) or LPT1-KO vs. WT strains (**c**). The experiments were done in two independent batches delimited by the vertical grey lines. (**d-e**) Distribution of the lipid classes (**d**) and fatty acyl groups (**e**) of the HcLPT1 and ScLPT1 products. *$p \leq 0.05$ by Fisher's exact test.

Fig. 4 | Fatty acid metabolism in *Histoplasma capsulatum*. (**a**) Distribution of carbon chain lengths of fatty acyl groups from lipids in global lipidomic analysis. (**b**) Fatty acid desaturase pathways in *H. capsulatum*, *Saccharomyces cerevisiae* and Human. (**c**) Distribution of double bonds on fatty acyl groups from lipids in global lipidomic analysis. (**d**) Minimum inhibitory concentrations (MIC) of fatty acid desaturase inhibitors. The MICs were obtained from 5 independent experiments with 4 replicates each. (**e**) Effect of fatty acid desaturase inhibitors in the fatty acid profile. Cells were grown in one half of each compound MIC and submitted to fatty acid analysis. The values represent the ratio of peak areas of unsaturated/saturate fatty acids. Statistical tests: *$p \leq 0.05$ by Fisher's exact test and # $p \leq 0.05$ by Student *t*-test.

Fig. 5 | Sphingolipid metabolism in *Histoplasma capsulatum*. (**a**) Sphingolipids of *H. capsulatum*, *Saccharomyces cerevisiae* and Human. (**b**) Minimum inhibitory concentration (MIC) of myriocin, the inhibitor of serine-palmitoyl transferase, which is the first step of the sphingolipid biosynthesis. The MICs were obtained from 5 independent experiments with 4 replicates each. (**c**) Effect of myriocin on the lipidomics profile. Cells were grown in one half of myriocin MIC and submitted to fatty acid analysis. The values represent the mass spectral signal intensity on the apex of the peak. Statistical tests: *$p \leq 0.05$ by Fisher's exact test and # $p \leq 0.05$ by student *t*-test.

Fig. 6 | Identification and validation of platelet-activating factor (PAF) analogs in *Histoplasma capsulatum*. (**a**) Structure, monoisotopic mass and tandem mass (MS/MS) fragments of PAF and analogs. (**b**) LC-MS/MS analysis of *H. capsulatum* PC (16:0/2:0) against the synthetic standard. The graphs showed the same retention time of extracted ion chromatograms of *H. capsulatum* phospholipids, *H. capsulatum* phospholipids + standard and standard alone. (**c-d**) MS/MS spectrum (**c**) and ion mobility-mass spectrometry (IMS-MS) (**d**) analyses of the PC (16:0/2:0) compared to the synthetic standard. The MS/MS analysis show the diagnostic fragment of phosphatidylcholines at *m/z* 184.07 (**d**), whereas the IMS-MS shows that the molecule has compatible arrival time and collision cross sections (stated in $Å^2$) with the standard.

Fig. 7 | Effect of fractions enriched in *Histoplasma capsulatum* PAF analogs in platelet aggregation. Human peripheral blood was incubated with the indicated positive controls and fractions enriched in *H. capsulatum* PAF analogs and aggregation was measured under an aggregometer. Panels **a** and **b** are two measurements of platelet aggregation activity of HPLC fractions enriched with *H. capsulatum* PAF analogs (fractions 8-10). The arrows indicate the addition of each compound or HPLC fraction. The figure is representative of two independent experiments with similar results.

Fig. 8 | Cytokine production by J774 macrophages stimulated with HPLC fractions enriched in *Histoplasma capsulatum* PAF analogs. J774 macrophages were pre-treated or not with the PAF receptor antagonist (WEB2086 – 10 mM) for 30 minutes before the incubation with acyl-PAF PC (16:0/2:0) and HPLC fractions enriched in *H. capsulatum* PAF analogs (fractions 9-10) for 24 hours. After the incubation period, TNF-α (**a**) and IL-10 (**b**) were quantified from the cell culture supernatants by ELISA. The graphs show averages and SEM for 3 experiments. The analysis reviewed an induction of cytokine production by HPLC fractions

enriched in *H. capsulatum* PAF analogs, which were inhibited by the PAF receptor agonist WEB2086 (WEB). *$p < 0.05$ for groups compared to the solvent control (first bar). +$p < 0.05$ for respective groups in the presence and absence of WEB2086 by ANOVA followed by Tukey's multiple comparison test.

Legends of supplementary figures and tables

Supplementary fig. 1 | Tandem-mass (MS/MS) spectra of the platelet-activating factor analog PC(16:2/2:0). Abbreviations: Ac, acetate; Cho, choline; ChoP, phosphocholine; ChoPGlyc; glycerophosphocholine; CID, collision-induced dissociation; DG, diacylglycerol; HCD, high-energy induced dissociation; M, mass; m/z, mass-over-charge ratio; ppm, parts-per-million. The spectra show diagnostic fragments for phosphatidylcholine (Cho, ChoP and ChoPGlyc) and for an acetyl group (M-Ac-H_2O).

Supplementary fig. 2 | Tandem-mass (MS/MS) spectra of the platelet-activating factor analog PC(16:1/2:0). Abbreviations: Ac, acetate; Cho, choline; ChoP, phosphocholine; ChoPGlyc; glycerophosphocholine; CID, collision-induced dissociation; DG, diacylglycerol; HCD, high-energy induced dissociation; LPA, lysophosphatidic acid; M, mass; m/z, mass-over-charge ratio; ppm, parts-per-million. The spectra show diagnostic fragments for phosphatidylcholine (Cho, ChoP and ChoPGlyc) and for an acetyl group (M-Ac-H_2O and LPA(16:1)-H_2O).

Supplementary fig. 3 | Quantification of PC(16:1/2:0) in wild-type (WT) and *Lpt1*-knockout (KO) *Saccharomyces cerevisiae* strains transformed with a plasmid containing the *Histoplasma capsulatum Lpt1* gene (pHcLPT1). *S. cerevisiae* strains complemented or not with the pESC-URA plasmid with Hc-LPT1 gene under galactose-inducible promoter and grown in YNB medium supplemented with galactose. The experiment was performed with 4 replicates. Statistical test was done with student *t*-test considering equal distribution.

Supplementary tab. 1 | List of identified lipids in the global lipidomics analysis.

Supplementary tab. 2 | Quantification of identified lipids in the positive mode of global lipidomics analysis. The quantitative information is based on the extracted intensity of each lipid species at the peak apex. The measurements were performed in 4 replicates.

Supplementary tab. 3 | Quantification of identified lipids in the positive mode of global lipidomics analysis. The quantitative information is based on the extracted intensity of each lipid species at the peak apex. The measurements were performed in 4 replicates.

Supplementary tab. 4 | List of identified lipids in the phospholipidomics analysis.

Supplementary tab. 5 | Quantification of identified lipids in the positive mode of phospholipidomics analysis. The quantitative information is based on the extracted intensity of each lipid species at the peak apex. The measurements were performed in 4 replicates.

Supplementary tab. 6 | Quantification of identified lipids in the positive mode of phospholipidomics analysis. The quantitative information is based on the extracted intensity of each lipid species at the peak apex. The measurements were performed in 4 replicates.

Supplementary tab. 7 | Quantification of identified sterol species in the gas chromatography-mass spectrometry analysis. The quantitative information is based on the extracted peak areas of each lipid species. The measurements were performed in 4 replicates.

Supplementary tab. 8 | Quantification of identified fatty acid species in the gas chromatography-mass spectrometry analysis. The quantitative information is based on the extracted peak areas of each lipid species. The measurements were performed in 4 replicates.

Supplementary tab. 9 | Quantification of identified proteins in the proteomics analysis. The quantitative information is based on the intensity based absolute quantification method (iBAQ), which was further converted to relative copy number of proteins per cell.

Supplementary tab. 10 | List of orthologues from *Saccharomyces cerevisiae* S288c and *Cryptococcus neoformans* H99 to *Histoplasma capsulatum* G186AR.

Supplementary tab. 11 | Lipid species upregulated in *Saccharomyces cerevisiae* strains expressing the *Histoplasma capsulatum Lpt1* gene. The analysis was done in wild-type (WT) and LPT1-knockout (KO) *S. cerevisiae* strains complemented or not with the pESC-URA plasmid with Hc-LPT1 gene under galactose-inducible promoter. *S. cerevisiae* WT and LPT1-knockout strains were grown in YNB medium supplemented with of glucose (Glc) or galactose (Gal). The measurements were performed in 4 replicates. Statistical analysis was down with student *t*-test considering equal distribution.

Supplementary tab. 12 | Lipid species downregulated in *Saccharomyces cerevisiae* strains expressing the *Histoplasma capsulatum Lpt1* gene. The analysis was done in wild-type (WT) and LPT1-knockout (KO) *S. cerevisiae* strains complemented or not with the pESC-URA plasmid with Hc-LPT1 gene under galactose-inducible promoter. *S. cerevisiae* WT and LPT1-knockout strains were grown in YNB medium supplemented with of glucose (Glc) or galactose (Gal). The measurements were performed in 4 replicates. Statistical analysis was down with student *t*-test considering equal distribution.

Supplementary tab. 13 | Lipid species downregulated in *Saccharomyces cerevisiae Lpt1* knockout strain. The analysis was done in wild-type and LPT1-knockout (KO) strains grown in YNB medium supplemented with of glucose (Glc) or galactose (Gal). The measurements were performed in 4 replicates. Statistical analysis was down with student *t*-test considering equal distribution.

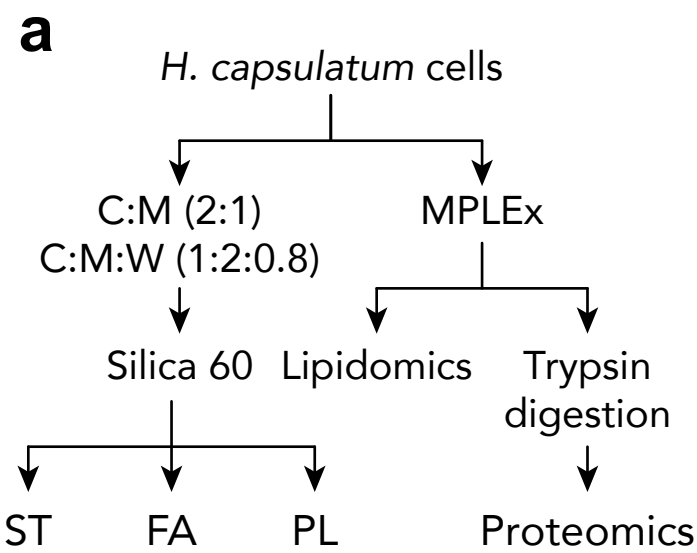

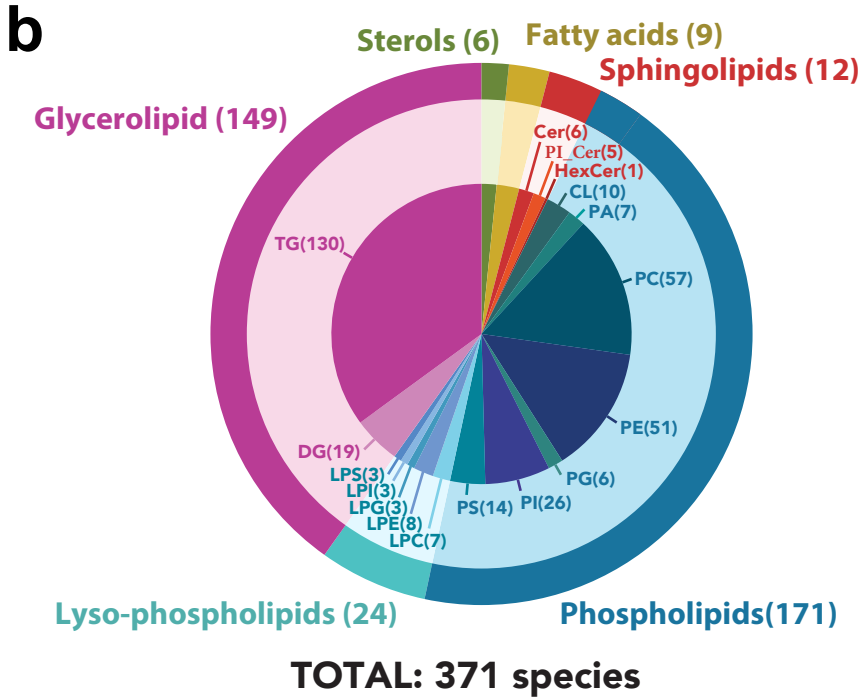

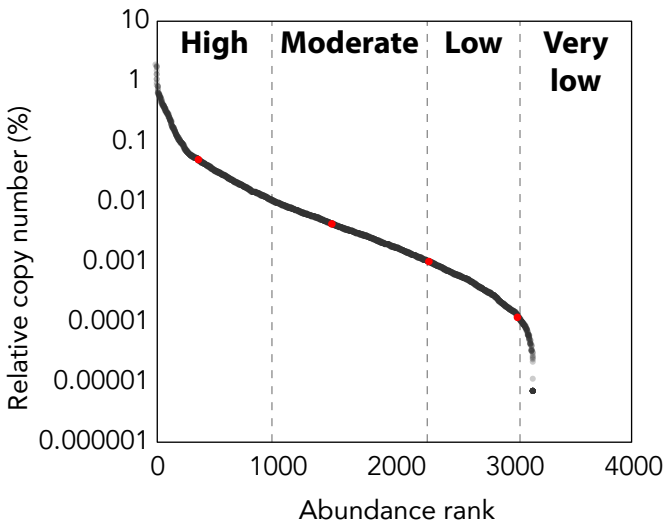

d

Pathway	Fold Enrichment High	Moderate	Low	Very Low
Glycolysis / Gluconeogenesis	**5.9**	1.1	0.0	0.0
Citrate cycle (TCA cycle)	**8.7**	0.0	0.0	0.0
DNA replication	1.3	**3.9**	**2.4**	2.3
Nicotinate and nicotinamide metabolism	0.6	1.7	**4.1**	0.0
Basal transcription factors	0.3	**2.4**	**4.4**	**7.0**
Fatty acid metabolism	**4.5**	1.6	0.4	0.0
Fatty acid biosynthesis	**3.8**	1.4	0.0	0.0
Fatty acid elongation	**4.7**	1.8	1.5	0.0
Fatty acid degradation	**5.5**	1.2	0.0	0.0
Arachidonic acid metabolism	4.7	0.0	0.0	0.0
alpha-Linolenic acid metabolism	1.6	1.2	0.0	0.0
Biosynthesis of unsaturated fatty acids	**3.1**	1.8	0.0	0.0
Steroid biosynthesis	1.7	**2.9**	1.6	0.0
Glycerophospholipid metabolism	0.5	**2.2**	**2.7**	3.4
Ether lipid metabolism	0.9	0.6	**6.4**	0.0
Sphingolipid metabolism	1.4	2.2	1.8	0.0
Glycosylphosphatidylinositol (GPI)-anchor biosynthesis	0.0	1.5	1.2	0.0

Fig. 1

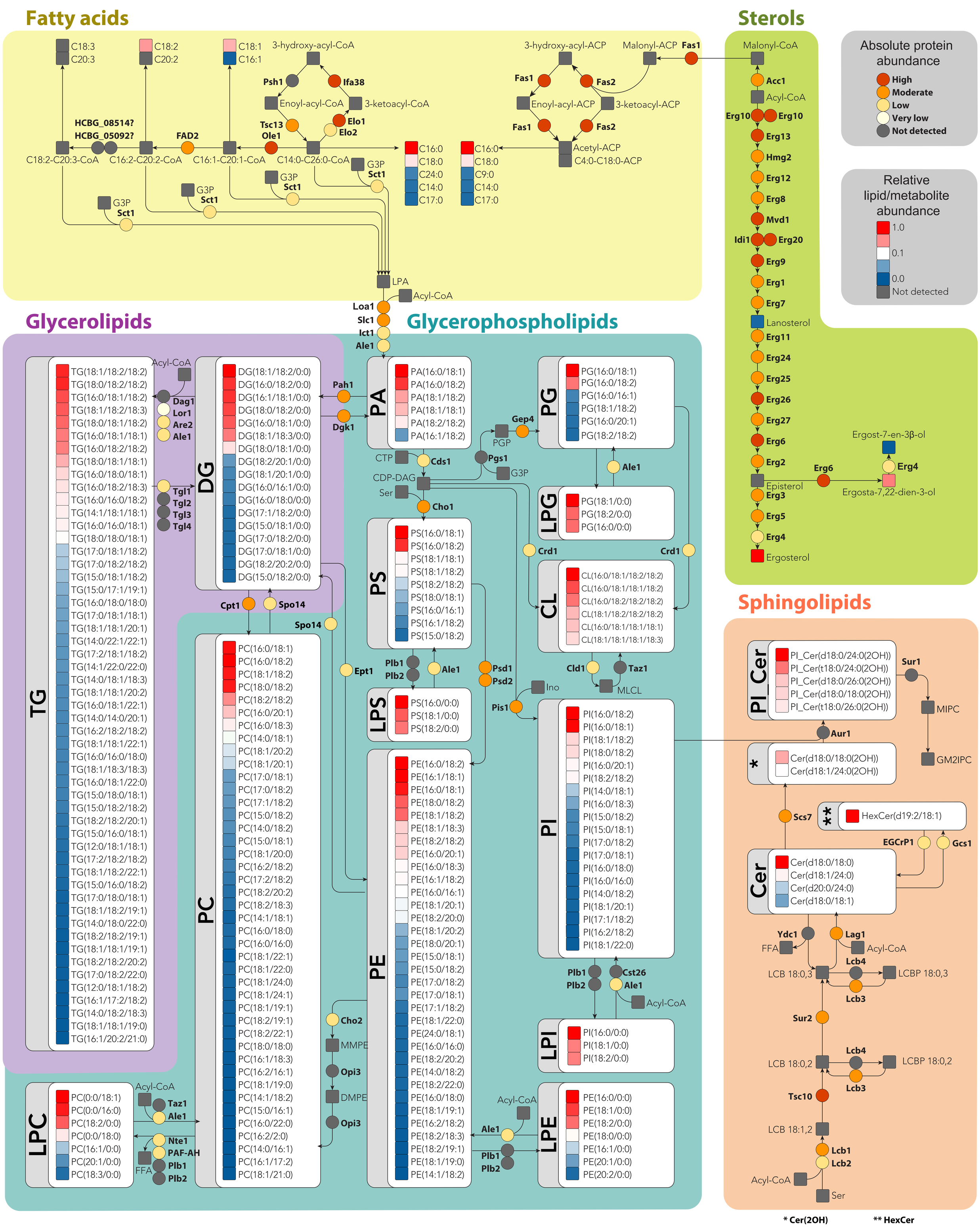
Fatty acids
Sterols
Glycerolipids
Glycerophospholipids
Sphingolipids
Absolute protein abundance
High
Moderate
Low
Very low
Not detected
Relative lipid/metabolite abundance
1.0
0.1
0.0
Not detected
C18:3
C20:3
C18:2
C20:2
C18:1
C16:1
3-hydroxy-acyl-CoA
Psh1
Ifa38
Enoyl-acyl-CoA
3-ketoacyl-CoA
Tsc13
Ole1
Elo1
Elo2
HCBG_08514?
HCBG_05092?
FAD2
C18:2-C20:3-CoA
C16:2-C20:2-CoA
C16:1-C20:1-CoA
C14:0-C26:0-CoA
G3P
Sct1
C16:0
C18:0
C24:0
C14:0
C17:0
3-hydroxy-acyl-ACP
Malonyl-ACP
Fas1
Fas2
Enoyl-acyl-ACP
3-ketoacyl-ACP
Acetyl-ACP
C4:0-C18:0-ACP
C9:0
Malonyl-CoA
Acc1
Acyl-CoA
Erg10
Erg13
Hmg2
Erg12
Erg8
Mvd1
Idi1
Erg20
Erg9
Erg1
Erg7
Lanosterol
Erg11
Erg24
Erg25
Erg26
Erg27
Erg6
Erg2
Episterol
Erg3
Erg5
Erg4
Ergosterol
Ergost-7-en-3β-ol
Ergosta-7,22-dien-3-ol
LPA
Loa1
Slc1
Ict1
Ale1
TG
TG(18:1/18:2/18:2)
TG(18:0/18:2/18:2)
TG(16:0/18:1/18:2)
TG(18:1/18:2/18:3)
TG(18:0/18:1/18:2)
TG(16:0/18:1/18:1)
TG(16:0/18:2/18:2)
TG(18:0/18:1/18:1)
TG(16:0/18:0/18:1)
TG(16:0/18:2/18:3)
TG(16:0/16:0/18:2)
TG(14:1/18:1/18:1)
TG(16:0/16:0/18:1)
TG(18:0/18:0/18:1)
TG(17:0/18:1/18:2)
TG(17:0/18:2/18:2)
TG(15:0/18:1/18:2)
TG(15:0/17:1/19:1)
TG(16:0/18:0/18:0)
TG(17:0/18:1/18:1)
TG(18:1/18:1/20:1)
TG(14:0/22:1/22:1)
TG(17:2/18:1/18:2)
TG(14:1/22:0/22:0)
TG(14:0/18:1/18:3)
TG(18:1/18:1/20:2)
TG(16:0/18:1/22:1)
TG(14:0/14:0/20:1)
TG(16:2/18:2/18:2)
TG(18:1/18:1/22:1)
TG(16:0/16:0/18:0)
TG(18:1/18:3/18:3)
TG(16:0/18:1/22:0)
TG(15:0/18:0/18:1)
TG(15:0/18:2/18:2)
TG(18:2/18:2/20:1)
TG(15:0/16:0/18:1)
TG(12:0/18:1/18:1)
TG(17:2/18:2/18:2)
TG(18:1/18:2/22:1)
TG(15:0/16:0/18:2)
TG(17:0/18:0/18:1)
TG(18:1/18:2/19:1)
TG(14:0/18:0/22:0)
TG(18:2/18:2/19:1)
TG(18:1/18:1/19:1)
TG(18:2/18:2/20:2)
TG(17:0/18:2/22:0)
TG(12:0/18:1/18:2)
TG(16:1/17:2/18:2)
TG(14:0/18:2/18:3)
TG(18:1/18:1/19:0)
TG(16:1/20:2/21:0)
Acyl-CoA
Dag1
Lor1
Are2
Ale1
Tgl1
Tgl2
Tgl3
Tgl4
DG
DG(18:1/18:2/0:0)
DG(16:0/18:2/0:0)
DG(16:1/18:1/0:0)
DG(18:0/18:2/0:0)
DG(16:0/18:1/0:0)
DG(18:1/18:3/0:0)
DG(18:0/18:1/0:0)
DG(18:2/20:1/0:0)
DG(18:1/20:1/0:0)
DG(16:0/16:1/0:0)
DG(16:0/18:0/0:0)
DG(17:1/18:2/0:0)
DG(15:0/18:1/0:0)
DG(17:0/18:2/0:0)
DG(17:0/18:1/0:0)
DG(18:2/20:2/0:0)
DG(15:0/18:2/0:0)
Pah1
Dgk1
PA
PA(16:0/18:1)
PA(16:0/18:2)
PA(18:1/18:2)
PA(18:1/18:1)
PA(18:2/18:2)
PA(16:1/18:2)
CTP
Cds1
CDP-DAG
Ser
Cho1
PGP
Pgs1
G3P
Gep4
PG
PG(16:0/18:1)
PG(16:0/18:2)
PG(16:0/16:1)
PG(18:1/18:2)
PG(16:0/20:1)
PG(18:2/18:2)
Ale1
LPG
PG(18:1/0:0)
PG(18:2/0:0)
PG(16:0/0:0)
Crd1
CL
CL(16:0/18:1/18:2/18:2)
CL(16:0/18:1/18:1/18:2)
CL(16:0/18:2/18:2/18:2)
CL(18:1/18:2/18:2/18:2)
CL(16:0/18:1/18:1/18:1)
CL(18:1/18:1/18:1/18:3)
Cld1
Taz1
MLCL
Cpt1
Spo14
PC
PC(16:0/18:1)
PC(16:0/18:2)
PC(18:1/18:2)
PC(18:0/18:2)
PC(18:2/18:2)
PC(16:0/20:1)
PC(16:0/18:3)
PC(14:0/18:1)
PC(18:1/20:2)
PC(18:1/20:1)
PC(17:0/18:1)
PC(17:0/18:2)
PC(17:1/18:2)
PC(15:0/18:2)
PC(14:0/18:2)
PC(15:0/18:1)
PC(18:1/20:0)
PC(16:2/18:2)
PC(17:2/18:2)
PC(18:2/20:2)
PC(18:2/18:3)
PC(14:1/18:1)
PC(16:0/18:0)
PC(16:0/16:0)
PC(18:1/22:1)
PC(18:1/22:0)
PC(18:1/24:0)
PC(18:1/24:1)
PC(18:1/19:1)
PC(18:2/19:1)
PC(18:2/22:1)
PC(18:0/18:0)
PC(16:1/18:3)
PC(16:2/16:1)
PC(18:1/19:0)
PC(14:1/18:2)
PC(15:0/16:1)
PC(16:0/22:0)
PC(16:2/2:0)
PC(14:0/16:1)
PC(16:1/17:2)
PC(18:1/21:0)
Ept1
PS
PS(16:0/18:1)
PS(16:0/18:2)
PS(18:1/18:1)
PS(18:1/18:2)
PS(18:2/18:2)
PS(18:0/18:1)
PS(16:0/16:1)
PS(16:1/18:2)
PS(15:0/18:2)
Plb1
Plb2
LPS
PS(16:0/0:0)
PS(18:1/0:0)
PS(18:2/0:0)
Psd1
Psd2
Ino
Pis1
PE
PE(16:0/18:2)
PE(16:1/18:1)
PE(16:0/18:1)
PE(18:0/18:2)
PE(18:1/18:2)
PE(18:1/18:3)
PE(18:2/18:2)
PE(16:0/20:1)
PE(16:0/18:3)
PE(16:1/18:2)
PE(16:0/16:1)
PE(18:1/20:1)
PE(18:2/20:0)
PE(18:1/20:2)
PE(18:0/20:1)
PE(15:0/18:1)
PE(15:0/18:2)
PE(17:0/18:2)
PE(17:0/18:1)
PE(17:1/18:2)
PE(18:1/22:0)
PE(24:0/18:1)
PE(16:0/16:0)
PE(18:2/20:2)
PE(14:0/18:2)
PE(18:2/22:0)
PE(16:0/18:0)
PE(18:1/19:1)
PE(16:2/18:2)
PE(18:2/18:3)
PE(18:2/19:1)
PE(18:1/19:0)
PE(14:1/18:2)
Cho2
MMPE
Opi3
DMPE
Opi3
PI
PI(16:0/18:2)
PI(16:0/18:1)
PI(18:1/18:2)
PI(18:0/18:2)
PI(16:0/20:1)
PI(18:2/18:2)
PI(14:0/18:1)
PI(16:0/18:3)
PI(15:0/18:2)
PI(15:0/18:1)
PI(17:0/18:2)
PI(17:0/18:1)
PI(16:0/18:0)
PI(16:0/16:0)
PI(14:0/18:2)
PI(18:1/20:1)
PI(17:1/18:2)
PI(16:2/18:2)
PI(18:1/22:0)
Cst26
LPI
PI(16:0/0:0)
PI(18:1/0:0)
PI(18:2/0:0)
LPC
PC(0:0/18:1)
PC(0:0/16:0)
PC(18:2/0:0)
PC(0:0/18:0)
PC(16:1/0:0)
PC(20:1/0:0)
PC(18:3/0:0)
Taz1
Nte1
PAF-AH
FFA
LPE
PE(16:0/0:0)
PE(18:1/0:0)
PE(18:2/0:0)
PE(18:0/0:0)
PE(16:1/0:0)
PE(20:1/0:0)
PE(20:2/0:0)
PI_Cer
PI_Cer(d18:0/24:0(2OH))
PI_Cer(t18:0/24:0(2OH))
PI_Cer(d18:0/26:0(2OH))
PI_Cer(d18:0/18:0(2OH))
PI_Cer(t18:0/26:0(2OH))
Sur1
MIPC
GM2IPC
Aur1
*
Cer(d18:0/18:0(2OH))
Cer(d18:1/24:0(2OH))
Scs7
**
HexCer(d19:2/18:1)
EGCrP1
Gcs1
Cer
Cer(d18:0/18:0)
Cer(d18:1/24:0)
Cer(d20:0/24:0)
Cer(d18:0/18:1)
Ydc1
Lag1
LCB 18:0,3
Lcb4
LCBP 18:0,3
Lcb3
Sur2
LCB 18:0,2
LCBP 18:0,2
Tsc10
LCB 18:1,2
Lcb1
Lcb2
Ser
* Cer(2OH)
** HexCer

Fig. 2

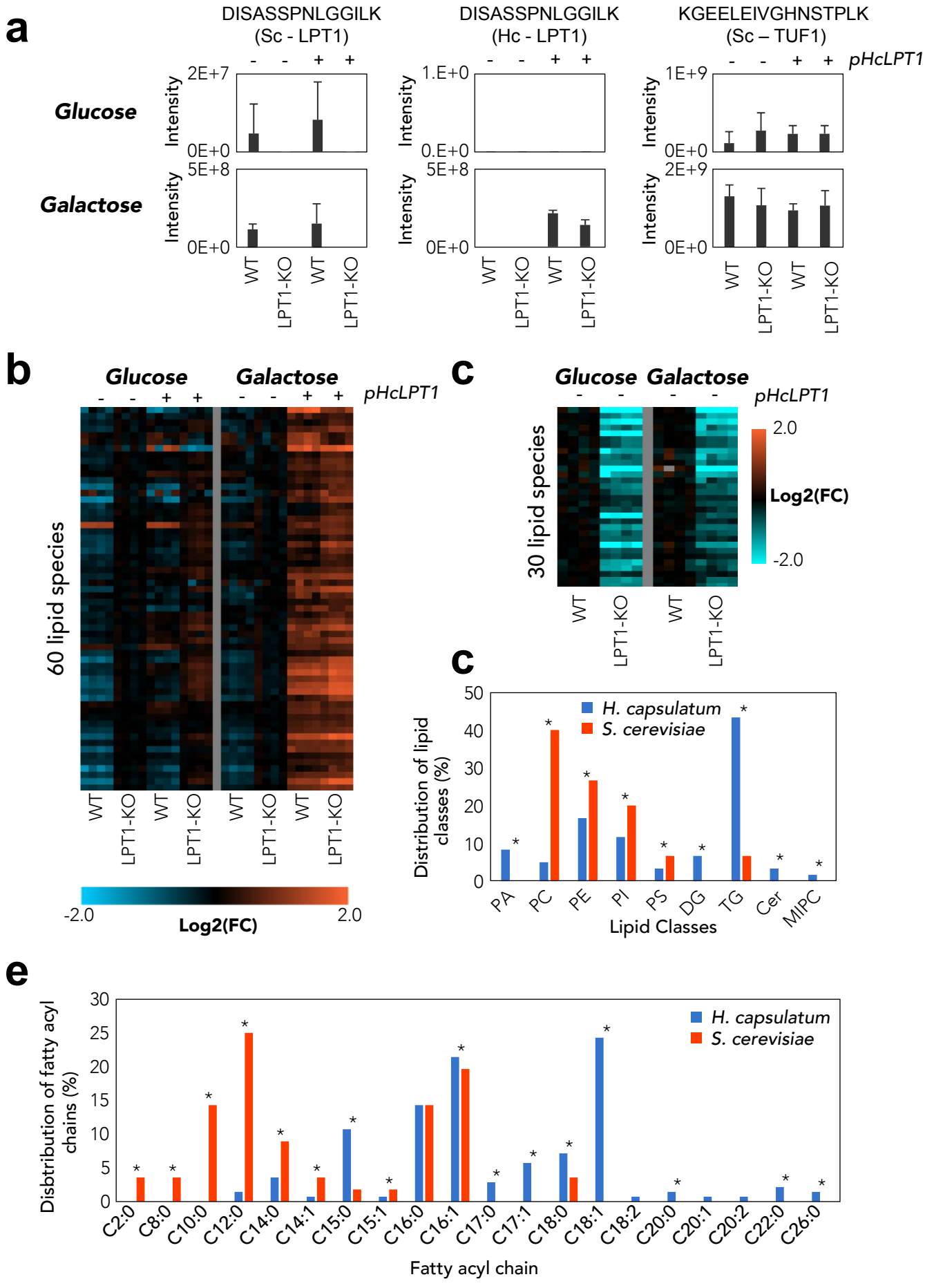
a
DISASSPNLGGILK
(Sc - LPT1)
DISASSPNLGGILK
(Hc - LPT1)
KGEELEIVGHNSTPLK
(Sc – TUF1)
pHcLPT1
Glucose
Galactose
Intensity
2E+7
0E+0
1.E+0
0.E+0
1E+9
5E+8
2E+9
WT
LPT1-KO
b
60 lipid species
-2.0
2.0
Log2(FC)
c
30 lipid species
c
Distribution of lipid classes (%)
H. capsulatum
S. cerevisiae
PA
PC
PE
PI
PS
DG
TG
Cer
MIPC
Lipid Classes
e
Disbtribution of fatty acyl chains (%)
C2:0
C8:0
C10:0
C12:0
C14:0
C14:1
C15:0
C15:1
C16:0
C16:1
C17:0
C17:1
C18:0
C18:1
C18:2
C20:0
C20:1
C20:2
C22:0
C26:0
Fatty acyl chain

Fig. 3

a

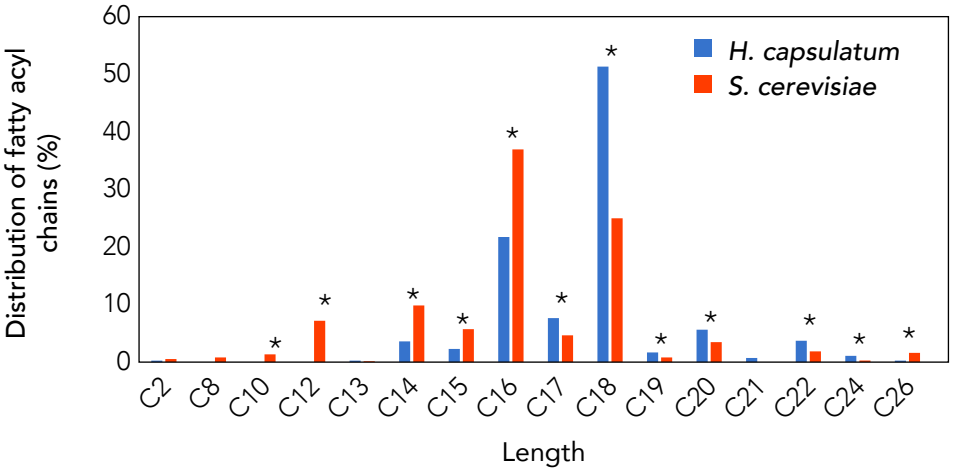

b

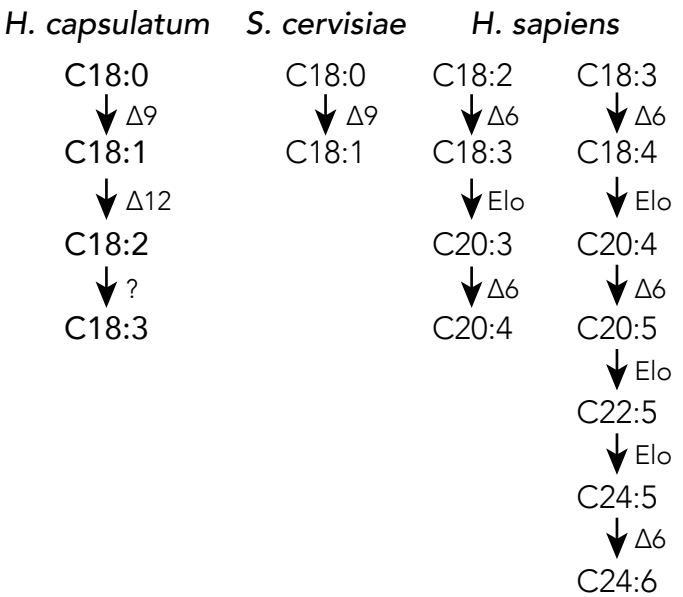

c

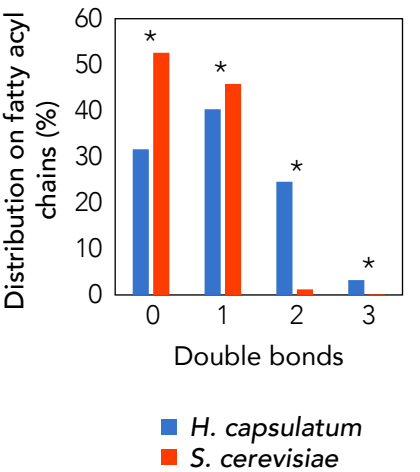

d

Drug	MIC (μM)
10-Thiastearic acid	1.25
Thiocarlide	12.5

e

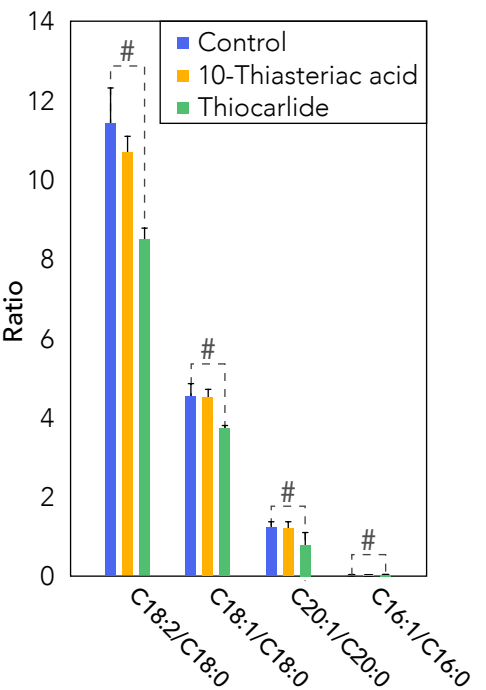

Fig. 4

a

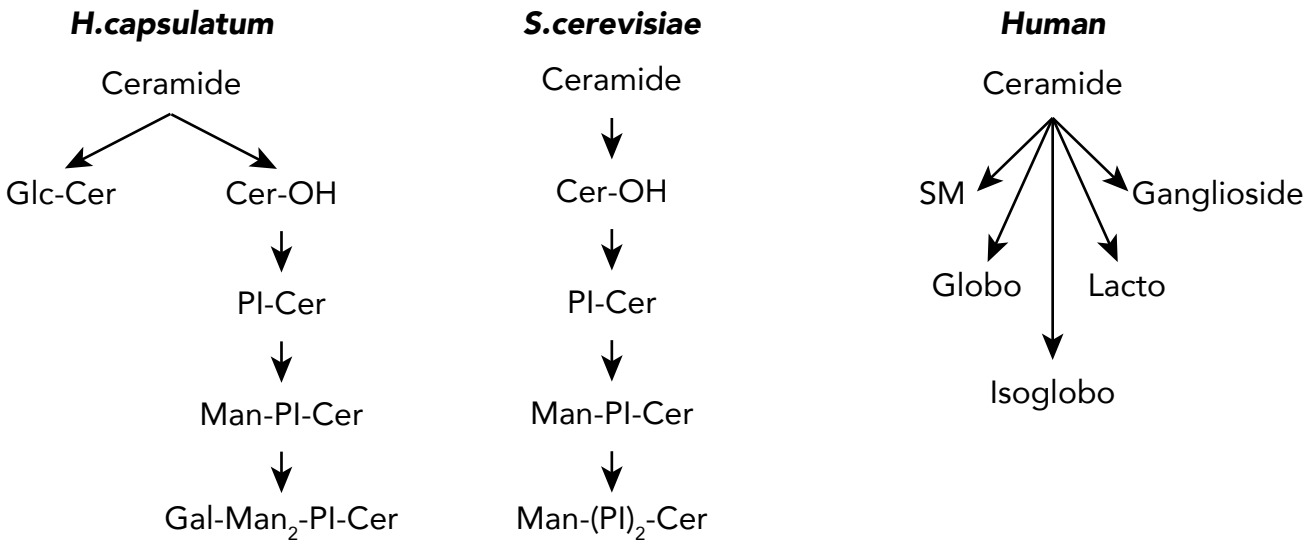

b

Drug	MIC (μM)
Myriocin	0.03

c

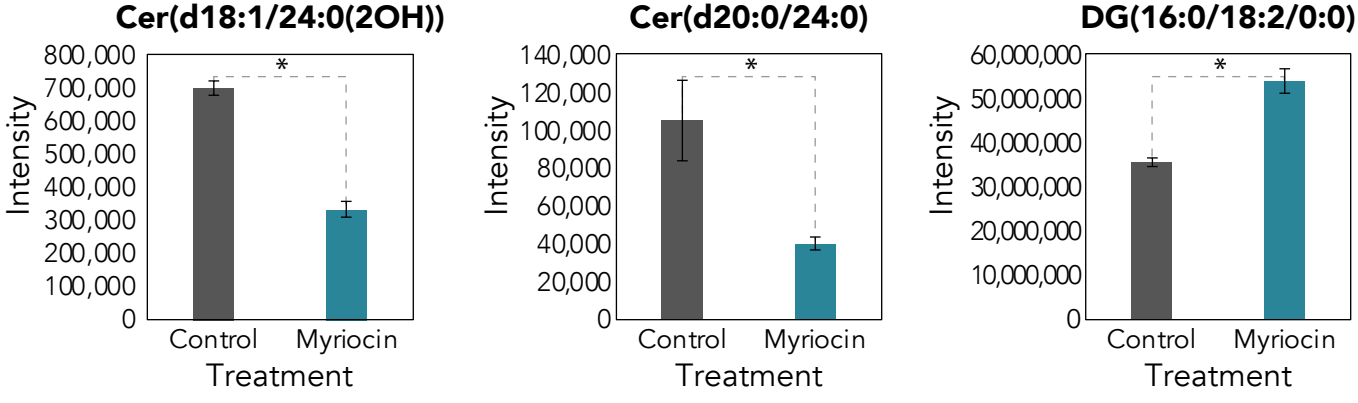

Fig. 5

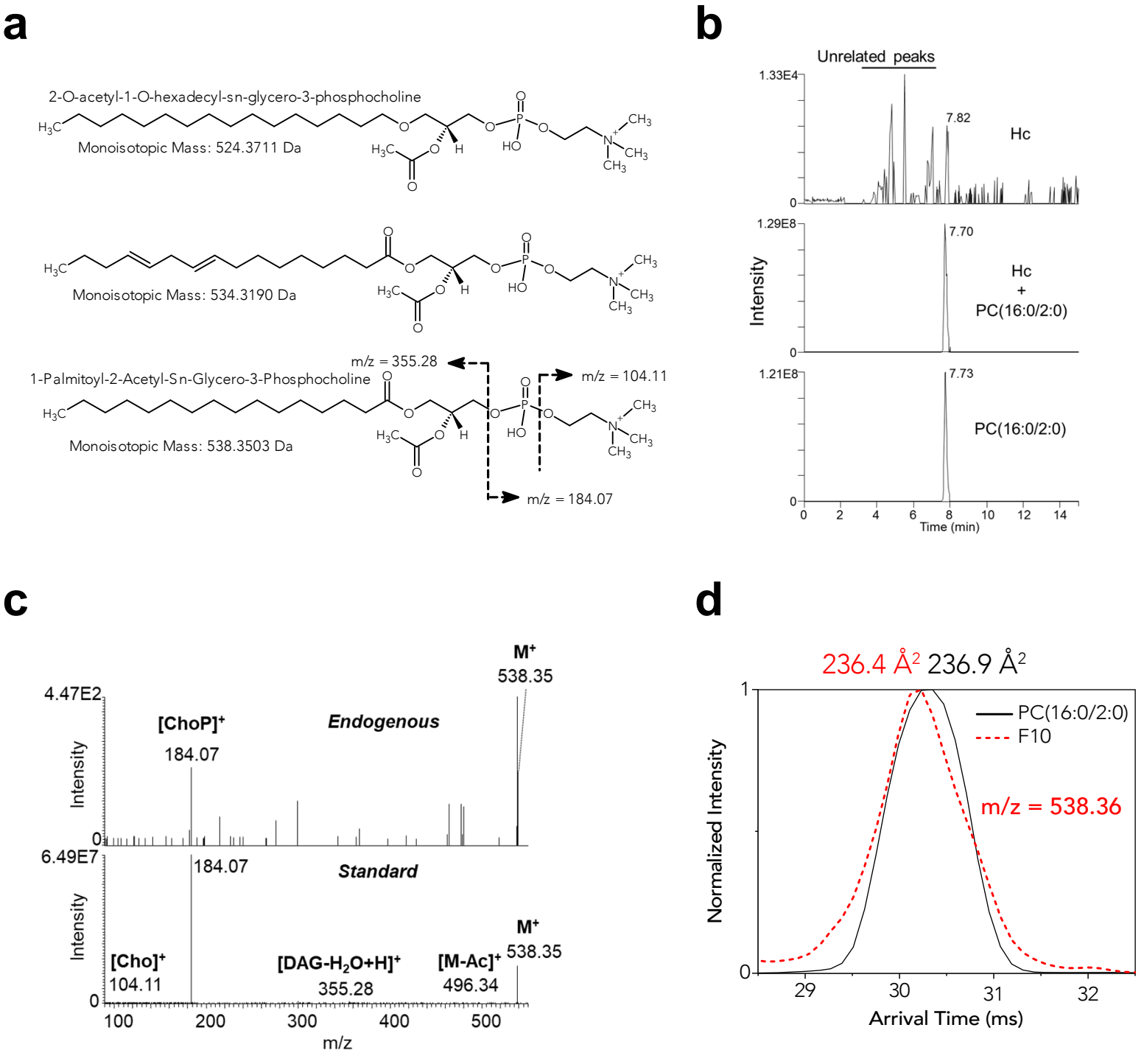
a
2-O-acetyl-1-O-hexadecyl-sn-glycero-3-phosphocholine
Monoisotopic Mass: 524.3711 Da
Monoisotopic Mass: 534.3190 Da
1-Palmitoyl-2-Acetyl-Sn-Glycero-3-Phosphocholine
Monoisotopic Mass: 538.3503 Da
m/z = 355.28
m/z = 104.11
m/z = 184.07
b
Unrelated peaks
1.33E4
7.82
Hc
1.29E8
7.70
Hc
+
PC(16:0/2:0)
1.21E8
7.73
PC(16:0/2:0)
Intensity
Time (min)
c
4.47E2
[ChoP]+
184.07
Endogenous
M+
538.35
6.49E7
184.07
Standard
[Cho]+
104.11
[DAG-H2O+H]+
355.28
[M-Ac]+
496.34
M+
538.35
Intensity
m/z
d
236.4 Å2 236.9 Å2
PC(16:0/2:0)
F10
m/z = 538.36
Normalized Intensity
Arrival Time (ms)

Fig. 6

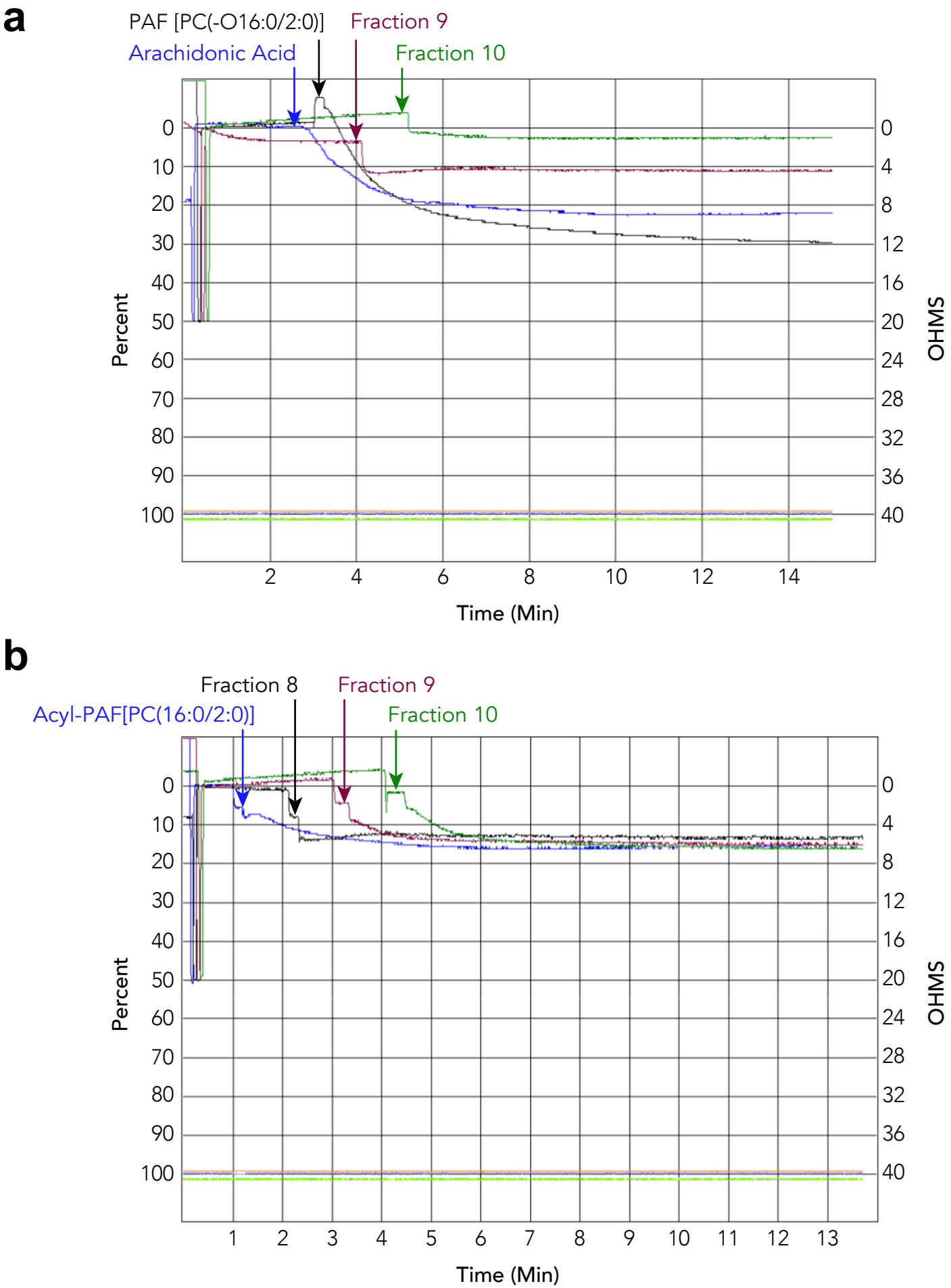
a
PAF [PC(-O16:0/2:0)]
Fraction 9
Arachidonic Acid
Fraction 10
Percent
OHMS
Time (Min)
b
Fraction 8
Fraction 9
Acyl-PAF[PC(16:0/2:0)]
Fraction 10
Percent
OHMS
Time (Min)

Fig. 7

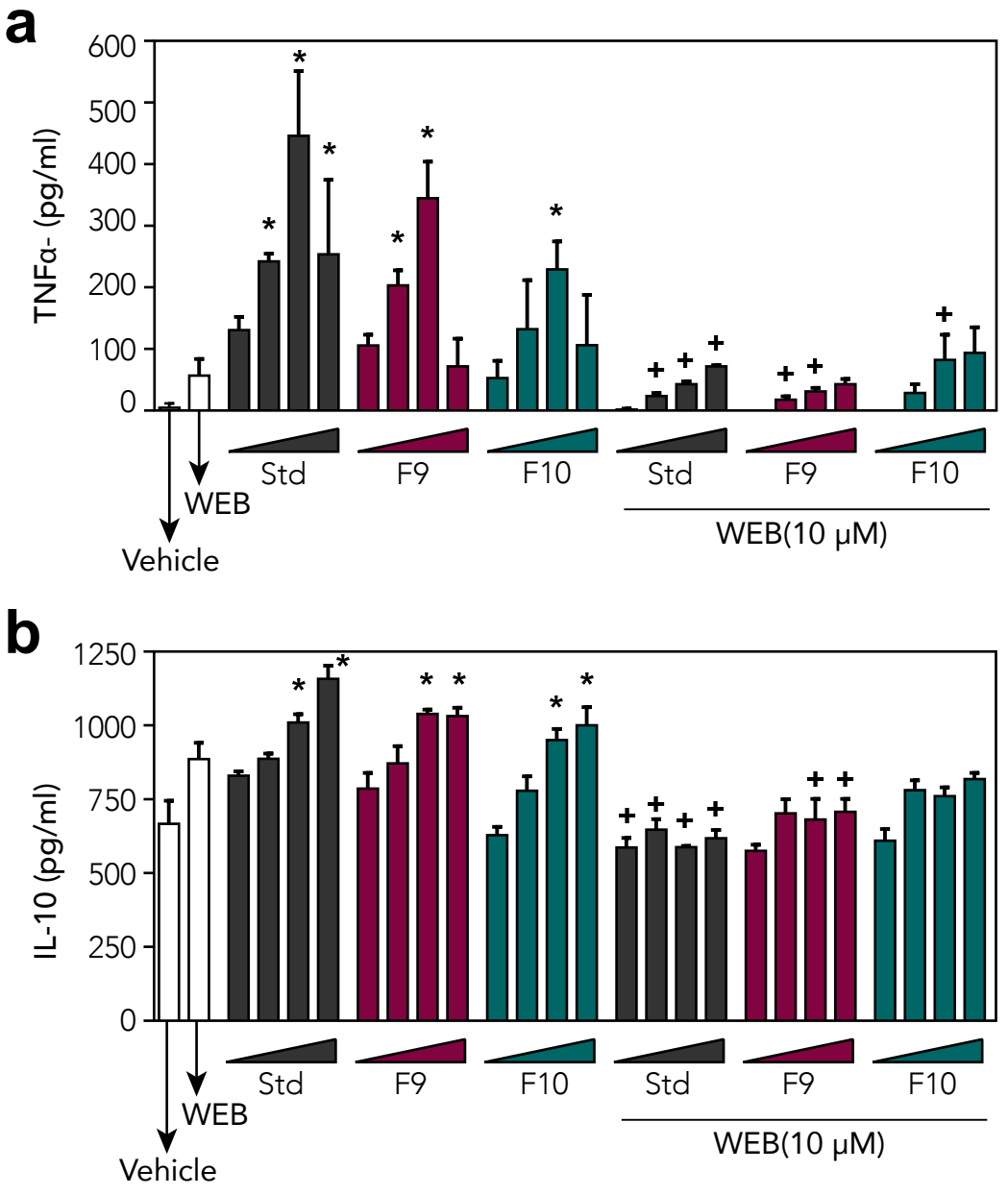
a
TNFα- (pg/ml)
600
500
400
300
200
100
0
Std
F9
F10
Std
F9
F10
WEB
Vehicle
WEB(10 μM)
b
IL-10 (pg/ml)
1250
1000
750
500
250
0
Std
F9
F10
Std
F9
F10
WEB
Vehicle
WEB(10 μM)

Fig. 8

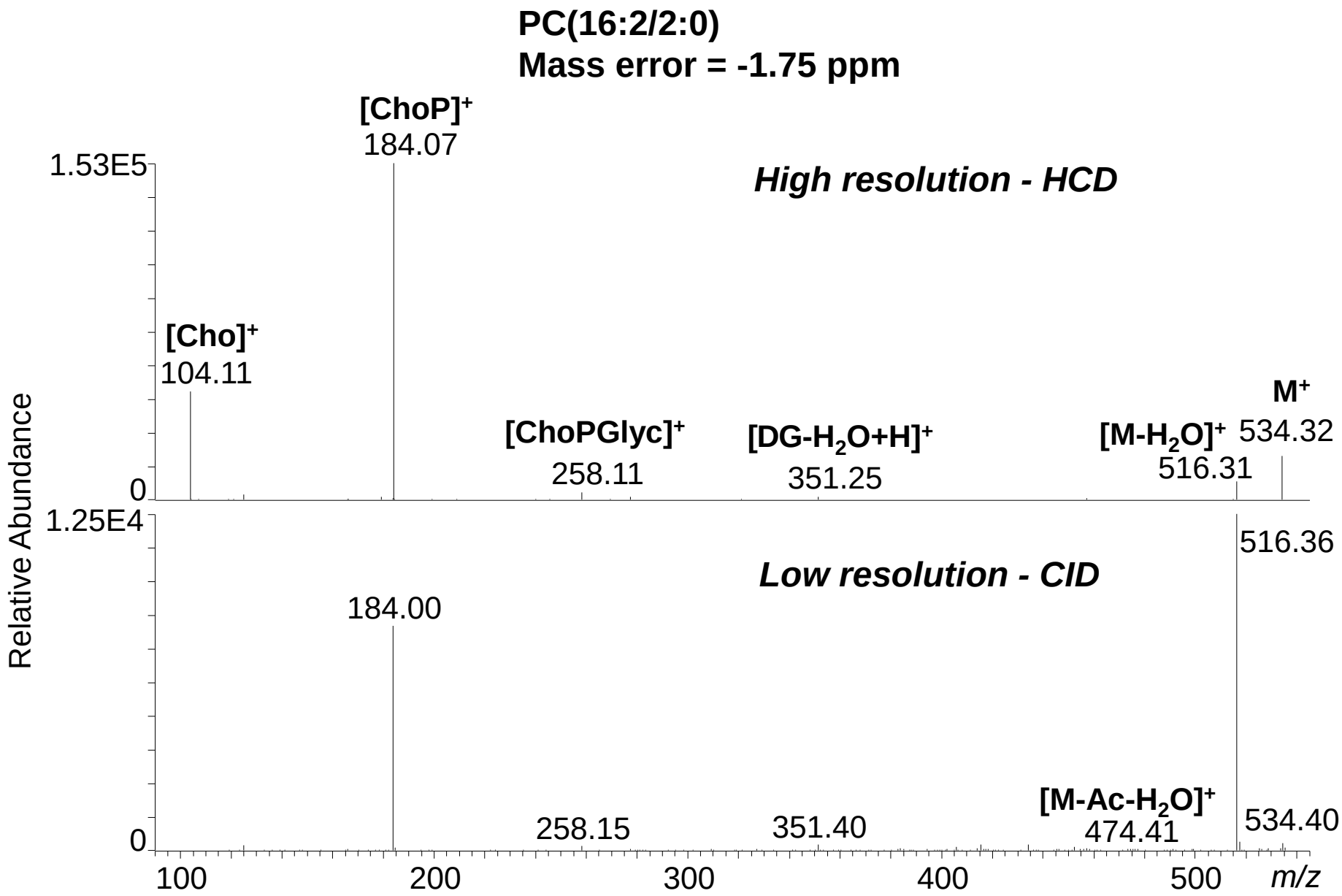

Supplementary fig. 1

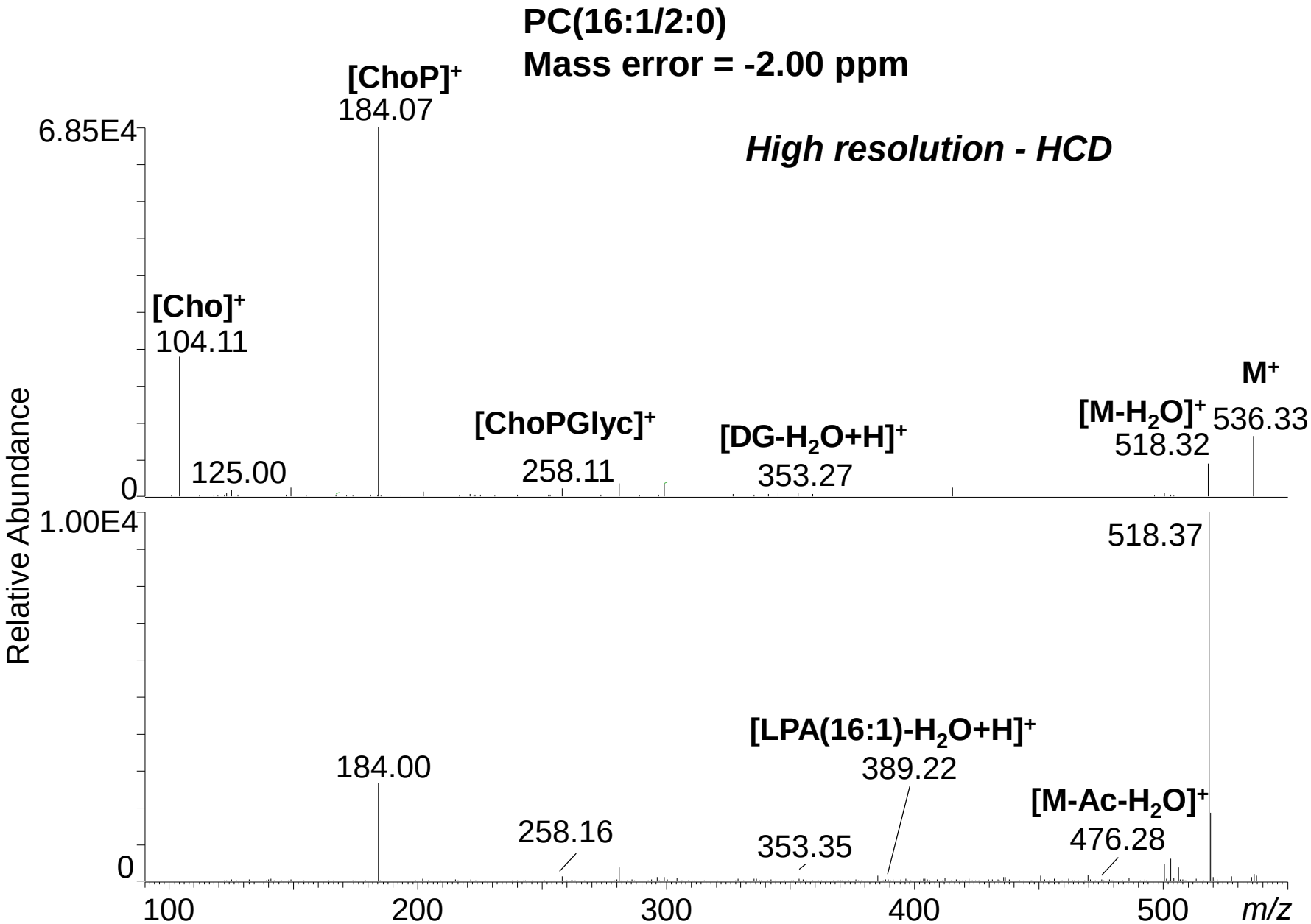

Supplementary fig. 2.

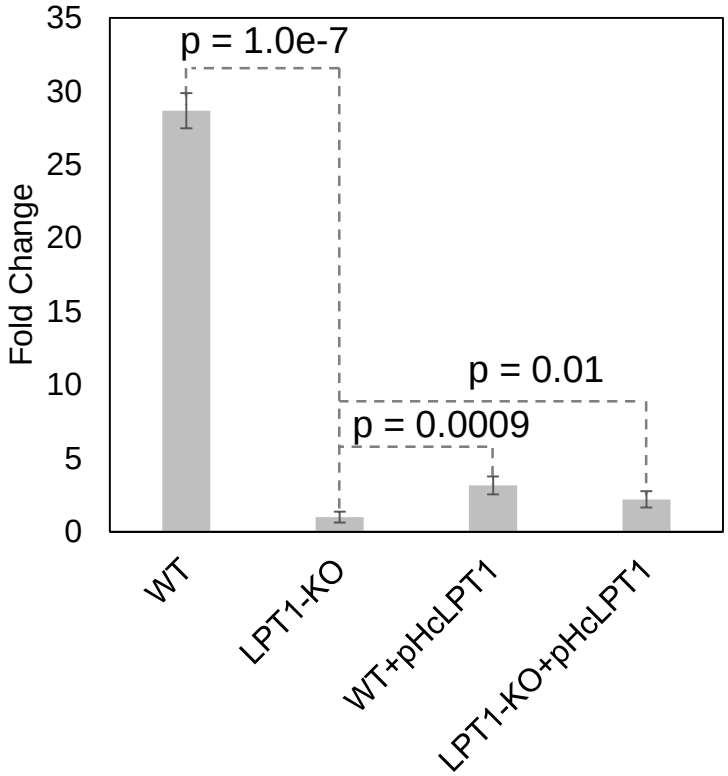

Supplementary fig. 3.